Turkish Journal of Earth Sciences

Manuscript 1913

Petrological and geochemical constraints on provenance, paleoweathering, and tectonic setting of the Cambro-Ordovician Khabour Formation, western and northern Iraq

ALI I. AL JUBOURY

MUHAMED F. OMER

MOHAMMED A. AL-HAJ

STEPHEN J. VINCENT

JAMES P. HOWARD

See next page for additional authors

Petrological and geochemical constraints on provenance, paleoweathering, and tectonic setting of the Cambro-Ordovician Khabour Formation, western and northern Iraq

Authors

ALI I. AL JUBOURY, MUHAMED F. OMER, MOHAMMED A. AL-HAJ, STEPHEN J. VINCENT, JAMES P. HOWARD, GARY NICHOLS, and BENOIT VAUTRAVERS

TÜBİTAK

Turkish Journal of Earth Sciences

http://journals.tubitak.gov.tr/earth/

Research Article

Turkish J Earth Sci
(2024) 33: 296-325

doi:10.55730/1300-0985.1913

Petrological and geochemical constraints on provenance, paleoweathering, and tectonic setting of the Cambro-Ordovician Khabour Formation, western and northern Iraq

Ali I. AL JUBOURY[1], Muhamed F. OMER[2,*], Mohammed A. AL HAJ[3], Stephen J. VINCENT[4], James P. HOWARD[4], Gary NICHOLS[5], Benoit VAUTRAVERS[4]

[1]Department of Petroleum Engineering, College of Engineering, Al Kitab University, Kirkuk, Iraq
[2]Department of Earth Sciences and Petroleum, Salahaddin University, Erbil, Iraq
[3]Geology Department, Mosul University, Mosul, Iraq
[4]CASP, West Building, Madingley Rise, Madingley Road, Cambridge, UK
[5]School of Environment and Technology, University of Brighton, Lewes Road, Brighton BN2 4GJ, UK

Received: 31.03.2023 • **Accepted/Published Online:** 16.01.2024 • **Final Version:** 19.03.2024

Abstract: Petrographic descriptions and point counting data, supported by SEM analysis, are presented for 89 sandstone samples of the Khabour Formation from the Khabour, Ora, Chalki Nasara, and Chia Zinnar outcrop sections in northern Iraq. These are compared with previously published data for subsurface samples from the Akkas-1 and Akkas-3 wells in western Iraq. Petrographic observations revealed that sublitharenites and subarkoses form the main sandstone types and may suggest a granitic source region with minor input from metamorphosed sediments. This is supported by the geochemical analysis gained from 66 sandstone samples. Chemical Index of Alteration (CIA) and Index of Chemical Variability (ICV) values along with A-CN-K trends, and Th/U versus Th relationships suggest moderate weathering and humid climatic conditions in the source area. The paleoclimate geochemical proxies are supported by clay mineral associations revealed by XRD and SEM data. Up-section trends in Rb/Sr values imply that humid and dry conditions prevailed during the deposition of the Khabour succession. The Khabour Formation sandstones were deposited in a passive margin setting; however, their ultimate origin is likely to be recycled orogen and continental block provenances with sTable craton sources and with uplifting in the basement complexes

Key words: Source area, tectonic setting, Khabour Formation, geochemical constraints, paleo-weathering

1. Introduction

The provenance and tectonic setting of siliciclastic rocks are commonly interpreted from the data gained from a combination of petrographic, mineralogic, and geochemical data (Dickinson, 1970; Dickinson and Suczek, 1979; Roser and Korsch, 1986; Pettijohn et al., 1987; Hussain et al., 2004; Zimmermann and Spalletti, 2009; Saydam Eker and Korkmaz, 2011; Al Juboury, 2012; Cao et al., 2012; Armstrong Altrin et al., 2012; Saydam Eker, 2012; Omer and Friis, 2014; Armstrong Altrin et al., 2015; Basu et al., 2016; Dai et al., 2016; Bessa et al., 2020; Cusack et al., 2020; Al Juboury et al., 2021; Jafarzadeh et al., 2022; Ghasemlooytakantapeh et al., 2023). Thus, the chemical and mineralogical chemical composition of siliciclastic sedimentary rocks is decisive in their provenance (Dickinson, 1970; Dickinson and Suczek, 1979; Saydam Eker and Korkmaz, 2011; Saydam Eker, 2012; Basu et al., 2016).

Additionally, the geochemical composition of siliciclastic sediments has been widely used to determine the degree of weathering of the source area (e.g., Nyakairu and Koeberl, 2001; Madhavaraju and Ramasamy, 2002; Al Juboury, 2012; Zhang et al., 2013; Rahman et al., 2014; Akkoca and Karatas, 2019; Omer et al., 2021). However, the components of clastic sedimentary rocks depend on several factors, such as weathering, recycling, transportation, deposition, and diagenesis. Many of these processes may have been repeated several times in the history of sedimentary rock, modifying most of the original features of its parent rock assemblage (McCann, 1991; Cox et al., 1995; Ghosh and Sarkar, 2010; Garzanti et al., 2013; Saydam Eker and Arı, 2020).

The Khabour Formation (Cambro–Ordovician) crops out in extreme northern Iraq and has been recorded from several wells in western Iraq. The thickest section drilled to date is 1913 m from the Akkas-1 well (Al Hadidy, 2007), whereas at its type section in the Khabour Valley, an 800 m thick section is exposed (Van Bellen et al., 1959; Blanc et al., 2012).

* Correspondence: muhamed.omer@su.edu.krd

The Khabour Formation consists of interbedded sandstone, shale, and claystone. Sandstone beds in the formation form hydrocarbon reservoirs in Iraq (Aqrawi et al., 2010; Al Juboury et al., 2019, Al Juboury et al., 2021). The shale units are also regarded as potential source rocks (Al Ameri and Baban, 2002; Al Juboury et al., 2020). The Silurian Akkas Formation overlies the Khabour Formation in subsurface sections from western Iraq, while in outcrop sections from extreme northern Iraq, the Khabour Formation is unconformably overlain by the Late Devonian Pirispiki Formation (Van Bellen et al., 1959).

The petrography and geochemistry of Khabour Formation sandstones in subsurface sections from western Iraq were described by Al Juboury et al. (2021) from the Akkas-1 and Akkas-3 wells to assess their reservoir characteristics and possible effects of Hirnantian glaciation. In the current work, petrographic descriptions along with geochemical results obtained from X-ray fluorescence (XRF) analysis and mineralogical X-ray diffraction (XRD) and scanning electron microscopy (SEM) were conducted. This study supplements these datasets with a suite of outcrop samples from four sections from the extreme northwest of Iraq. Together, these data are used to determine the provenance, paleoweathering and tectonic setting of the Khabour Formation in Iraq.

2. Geologic setting

During the early Paleozoic, Iraq was located at the northeastern passive margin of the Arabian Plate in northern Gondwana bordering the Paleo-Tethys Ocean to the north (Alavi, 1980; Sengör, 1990; Beydoun, 1991; Loosveld et al., 1996; Alavi, 2007; Ali et al., 2014). The thickness of the Paleozoic succession in Iraq ranges between 3–4 km based on seismic data (Aqrawi et al., 2010), however, its base has not been penetrated in wells and is not exposed at the surface.

The stratigraphy of Iraq has been influenced by its location between the Arabian part of Nubian–Arabian shield and the Asian branches of the Alpine tectonic belt and also by both regional and local deformation events. Structurally, Iraq was divided into five structural provinces by Buday and Jassim (1987), (Figure 1). The western part of Iraq comprises a sTable shelf, whilst extreme northern Iraq represents a thrust zone. During the Ordovician and Silurian, large areas of northern Gondwana were covered by shallow epeiric seas that bordered a low hinterland formed by the Nubian–Arabian shield (Husseini, 1990; McGillivray and Husseini, 1992; Beydoun, 1993; Sharland et al., 2001). Because the seas were shallow, their areal extent changed rapidly in response to eustatic sea-level change (Beydoun, 1991; Sharland et al., 2001). The coastline migrated over long distances resulting in great variation in the thickness and facies associations preserved on the platform (Numan, 1997; Konert et al., 2001).

Sharland et al. (2001) subdivided the stratigraphy of the Arabian plate into six tectonostratigraphic mega-sequences (TMS-AP1–6). The Early Cambrian to Late Ordovician succession (520–445 Ma), including the Khabour Formation, forms TMS-AP2 that has a duration of 75 Ma. During deposition of TMS-AP2, the intra-cratonic tectonic setting was dominated by extension and subsidence with a mild phase of tectonic uplift close to the Paleo-Tethys passive margin. At this time, Iraq was located at moderate to high southern latitudes and was dominated by clastic sedimentation (Husseini, 1992; McGillivray and Husseini, 1992; Al Fares et al., 1998). The top of mega-sequence TMS-AP2 corresponds to the top of the Khabour Formation; this represents a major sequence boundary on the Arabian Plate (Aqrawi, 1998; Sharland et al., 2001). This sequence boundary records a sea-level fall of 150–200 m (Haq et al., 1987) associated with the Hirnantian glaciation.

3. Materials and methods

In the current work, samples were analysed from sandstone units of the Khabour Formation from four outcrop sections in extreme northern Iraq (Ora, Khabour, Chalki Nasara and Chia Zinnar) (Figures 2 and 3). Additional data were also collected from samples from two studied wells originally described by Al Juboury et al. (2021) for reservoir quality assessement of the Khabour Formation in western Iraq. Eighty-nine sandstone samples from the four outcrop sections are described for the first time (Table 1). Petrographic data, obtained using a Nikon Microphot-FX petrographic microscope, were combined with that from 48 sandstone samples originally described by Al Juboury et al. (2021) from the Akkas-1 and Akkas-3 wells. Point-countingare summarised in Table 1. In order to minimize the dependence of rock composition on grain size, the Gazzi-Dickinson point-counting method was used (Ingersoll, et al., 1984), with 350 points per slide.

Representative SEM sample images were obtained using a F50/FEG SEM at Jordanian University, Amman, Jordan. XRD analysis for representative bulk samples was conducted at the Department of Earth Sciences, Royal Holloway University of London using a Philips X-ray diffractometer (PW3710). Peak identification was enabled using the Siroquant program.

Forty-six sandstone samples from three of the outcrop sections underwent XRF analysis (Tables 2 and 3) for major and trace elemental composition to make use of their distributions as proxies for provenance, paleoweathering and tectonic setting. A PANalytical Axios sequential X-ray fluorescence spectrometer was used for this analysis at Royal Holloway University of London. Sample preparation included two steps: Fused glass disc preparation and pressed pellet preparation. These are combined with 21 samples already analysed from the subsurface sections (Al Juboury et al., 2021).

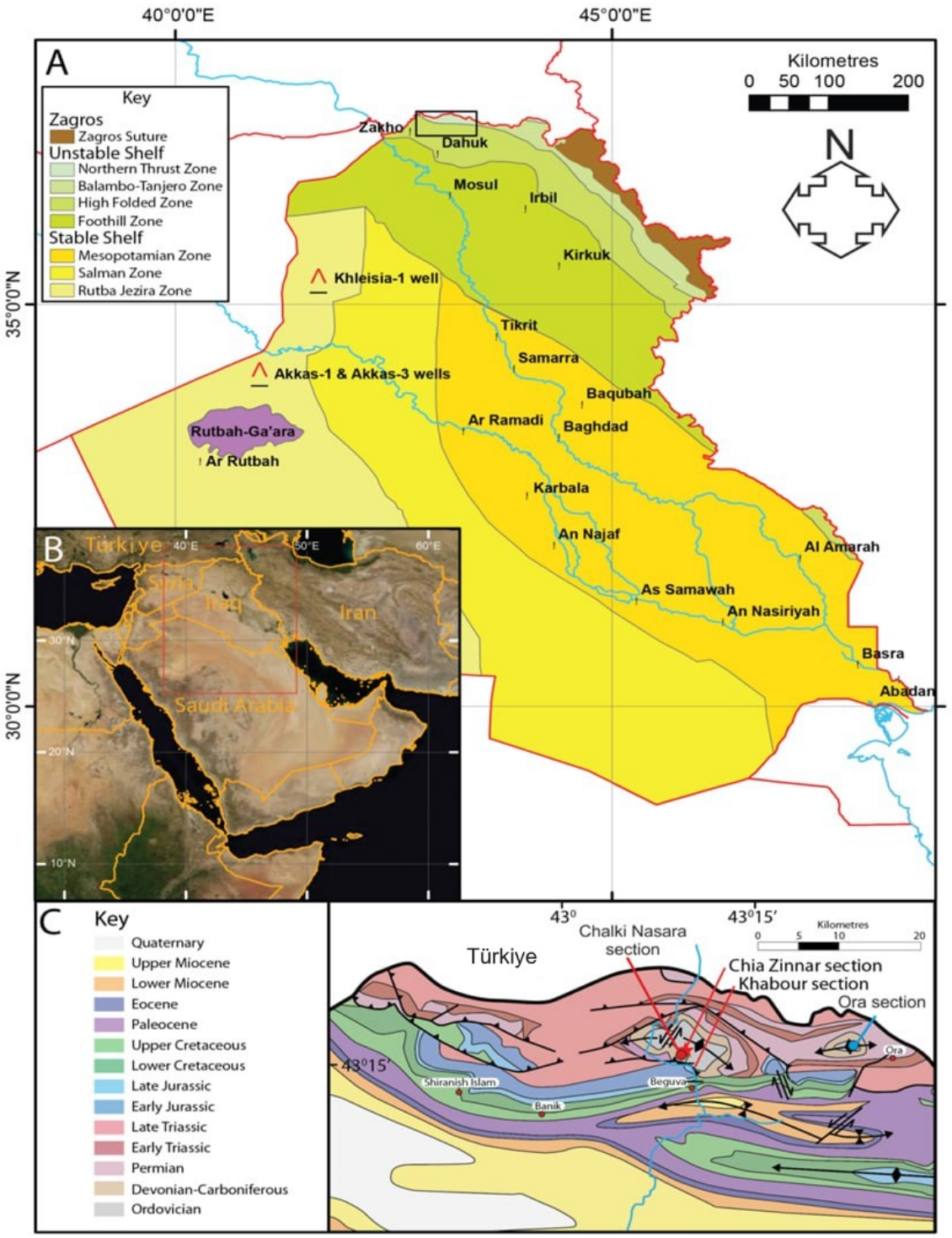

Figure 1. A- The structural provinces of Iraq (after Buday and Jassim, 1987), together with the locations of the Akkas-1 and Akkas-3 wells in western Iraq. B- Inset map shows the regional locations of Iraq and neighbouring countries; the main map is indicated by the red box. The black box shows the location of Khabour Formation outcrops in extreme northern Iraq. C- Geological map showing the studied sections of the Khabour Formation in northern Iraq (Sissakian, 2000).

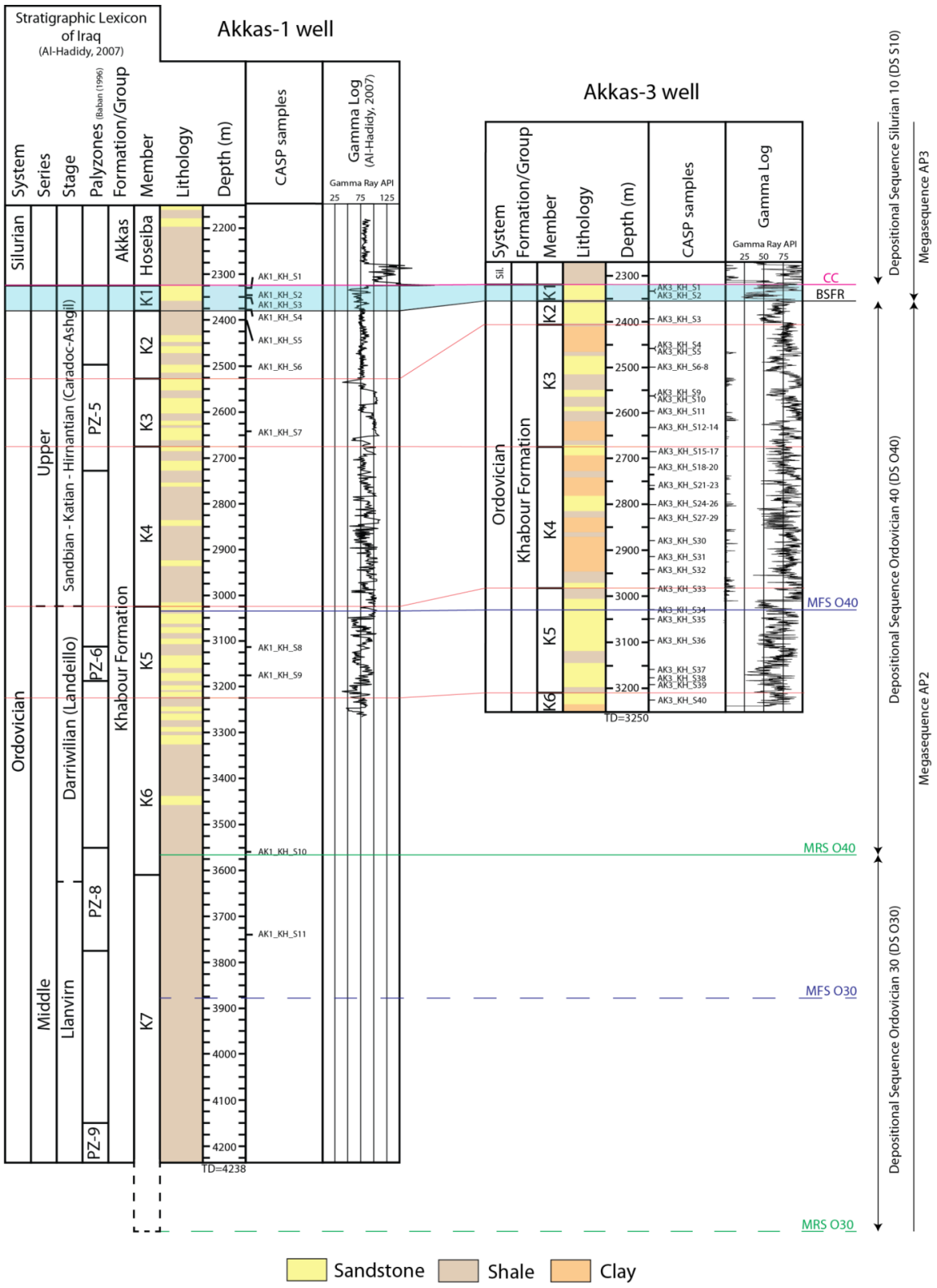

Figure 2. Lithologic sections for the Akkas-1 and Akkas-3 wells in western Iraq, with sample positions indicated (see Figure 1 for location).

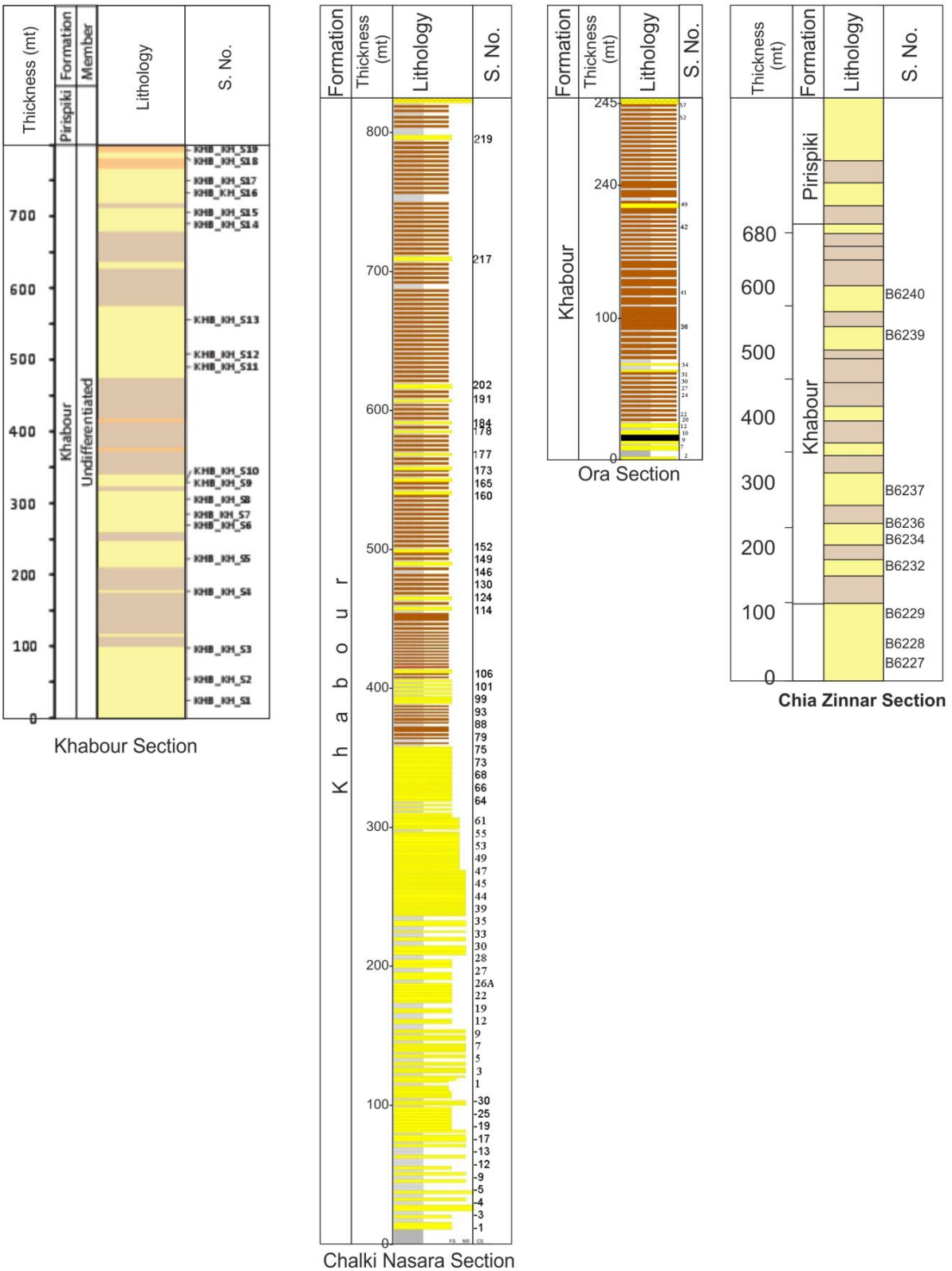

Figure 3. Lithologic sections from the surface outcrop sections (Khabour, Chalki Nasara, Ora and Chia Zinnar) from extreme northern Iraq with sample positions indicated (see Figure 1 for location).

Table 1. Point counting data for sandstones from the Khabour Formation from the studied sections. Data were collected using the Gazzi–Dickinson point counting technique. Data from the Akkas-1 and -3 wells were original documented in Al Juboury et al. (2021).

Section	Sample number	Quartz%	Feldspar%	Lithic grains %	Rock type
Akkas-1 well	**AK1_KH_S1**	85	13	2	Subarkose
	AK1_KH_S2	84	14	2	Subarkose
	AK1_KH_S3	88	10	2	Subarkose
	AK1_KH_S4	87	10	3	Subarkose
	AK1_KH_S5	87	12	1	Subarkose
	AK1_KH_S6	91	6	3	Subarkose
	AK1_KH_S7	90	9	1	Subarkose
	AK1_KH_S8	88	12	0	Subarkose
	AK1_KH_S9	84	15	1	Subarkose
	AK1_KH_S10	84	11	5	Subarkose
	AK1_KH_S11	87	11	2	Subarkose
Akkas-3 well	**AK3_KH_S1**	87	3	10	Sublitharenite
	AK3_KH_S2	91	4	5	Subarkose
	AK3_KH_S3	91	2	7	Sublitharenite
	AK3_KH_S4	88	5	7	Sublitharenite
	AK3_KH_S5	87	8	5	Subarkose
	AK3_KH_S6	93	3	4	Subarkose
	AK3_KH_S7	88	5	7	Sublitharenite
	AK3_KH_S8	86	9	5	Subarkose
	AK3_KH_S9	83	9	8	Subarkose
	AK3_KH_S10	88	3	9	Sublitharenite
	AK3_KH_S11	93	4	3	Subarkose
	AK3_KH_S12	88	5	7	Sublitharenite
	AK3_KH_S13	90	6	4	Sublitharenite
	AK3_KH_S14	85	10	5	Subarkose
	AK3_KH_S15	89	5	6	Sublitharenite
	AK3_KH_S17	87	6	7	Sublitharenite
	AK3_KH_S18	91	3	6	Sublitharenite
	AK3_KH_S19	87	5	8	Sublitharenite
	AK3_KH_S20	95	2	3	Subarkose
	AK3_KH_S22	88	5	7	Sublitharenite
	AK3_KH_S23	86	6	8	Sublitharenite
	AK3_KH_S24	89	5	6	Sublitharenite
	AK3_KH_S25	82	11	7	Subarkose
	AK3_KH_S26	86	6	8	Sublitharenite
	AK3_KH_S28	87	5	8	Sublitharenite
	AK3_KH_S29	90	3	7	Sublitharenite
	AK3_KH_S30	91	3	6	Sublitharenite
	AK3_KH_S31	84	9	7	Subarkose
	AK3_KH_S32	88	5	7	Sublitharenite
	AK3_KH_S33	91	4	5	Sublitharenite
	AK3_KH_S34	89	4	7	Sublitharenite
	AK3_KH_S35	91	3	6	Sublitharenite
	AK3_KH_S36	83	7	10	Sublitharenite
	AK3_KH_S37	87	6	7	Sublitharenite
	AK3_KH_S38	88	6	6	Sublitharenite
	AK3_KH_S39	79	15	6	Subarkose
	AK3_KH_S40	83	8	9	Sublitharenite

Table 1. (Continued).

Ora	**2**	95	4	1	Subarkose
	7	97	2	1	Subarkose
	9	97	2	1	Subarkose
	10	87	10	3	Subarkose
	12	95	4	1	Subarkose
	22	89	8	3	Subarkose
	24	97	2	1	Subarkose
	27	93	6	1	Subarkose
	30	91	7	2	Subarkose
	31	86	11	3	Subarkose
	34	95	4	1	Subarkose
	36	95	1	4	Sublitharenite
	41	97	1	2	Subarkose
	42	98	1	1	Quartzarenite
	57	92	7	1	Subarkose
Chalki Nasara	**CH-N -1**	91	8	1	Subarkose
	CH-N -3	93	6	1	Subarkose
	CH-N -4	94	5	1	Subarkose
	CH-N -5	90	7	3	Sublitharenite
	CH-N -9	86	13	1	Subarkose
	CH-N -12	87	13	0	Subarkose
	CH-N -13	87	11	2	Subarkose
	CH-N -17	90	8	2	Sublitharenite
	CH-N -19	81	17	1	Subarkose
	CH-N -25	90	9	1	Subarkose
	CH-N -30	97	3	0	Quartzarenite
	CH-N 5	92	6	2	Subarkose
	CH-N 7	97	3	0	Subarkose
	CH-N 9	92	0	8	Sublitharenite
	CH-N 12	93	5	2	Subarkose
	CH-N 22	95	4	1	Subarkose
	CH-N 26A	93	6	1	Subarkose
	CH-N 28	91	8	1	Subarkose
	CH-N 30	98	2	0	Quartzarenite
	CH-N 33	95	4	1	Subarkose
	CH-N 39	94	4	2	Subarkose
	CH-N 45	93	7	0	Subarkose
	CH-N 53	96.8	2.3	0.7	quartzarenite
	CH-N 66	93	2	5	Sublitharenite
	CH-N 73	89	7	4	Sublitharenite
	CH-N 88	92	8	0	Subarkose
	CH-N 93	93	0	67	Sublitharenite
	CH-N 99	96	2	2	Subarkose
	CH-N 101	91	2	7	Sublitharenite
	CH-N 106	99	0	1	Quartzarenite
	CH-N 114	96	4	0	Subarkose
	CH-N 124	98	1	1	Quartzarenite
	CH-N 130	98	2	0	Quartzarenite
	CH-N 146	93	6	1	Subarkose
	CH-N 149	94	5	1	Subarkose
	CH-N 152	92	2	6	Sublitharenite

Table 1. (Continued).

	CH-N 160	96	2	2	Subarkose
	CH-N 165	91	8	1	Subarkose
	CH-N 173	94	5	1	Subarkose
	CH-N 177	97	2	1	Subarkose
	CH-N 178	96	3	1	Subarkose
	CH-N 184	91	6	3	Subarkose
	CH-N 191	98	1	1	Quartzarenite
	CH-N 202	92	7	1	Subarkose
	CH-N 217	93	5	2	Subarkose
	CH-N 219	92	1	7	Sublitharenite
Khabour	**KHB_KH_S1**	93	4	3	Subarkose
	KHB_KH_S2	92	8	0	Subarkose
	KHB_KH_S3	85	6	9	Sublitharenite
	KHB_KH_S4	83	8	9	Sublitharenite
	KHB_KH_S5	83	6	11	Sublitharenite
	KHB_KH_S6	87	6	7	Sublitharenite
	KHB_KH_S7	88	8	4	Subarkose
	KHB_KH_S8	88	5	7	Sublitharenite
	KHB_KH_S9	89	5	6	Sublitharenite
	KHB_KH_S10	87	3	10	Sublitharenite
	KHB_KH_S11	91	4	5	Sublitharenite
	KHB_KH_S12	84	8	8	Sublitharenite
	KHB_KH_S13	87	5	8	Sublitharenite
	KHB_KH_S14	84	6	10	Sublitharenite
	KHB_KH_S15	89	3	8	Sublitharenite
	KHB_KH_S16	93	2	5	Sublitharenite
	KHB_KH_S17	92	2	6	Sublitharenite
	KHB_KH_S18	92	1	7	Sublitharenite
	KHB_KH_S19	91	2	7	Sublitharenite
Chia Zinnar	**B6227**	86	13	1	Subarkose
	B6228	89	8	3	Subarkose
	B6229	86	11	3	Subarkose
	B6232	80	19	1	subarkose
	B6234	68	28	4	Lithic arkose
	B6236	50	48	2	Arkose
	B6237	71	24	5	Arkose
	B6239	64	34	2	Arkose
	B6240	63	36	1	Arkose

4. Results

4.1. Sandstone petrology

Petrographic investigation reveals that the outcrop and subsurface sandstones of the Khabour Formation out crop sections (Ora, Chalki Nasara, Khabour and Chia Zinnar) and subsurface (Akkas-1 and Akkas-3 wells) are mainly subarkoses and sublitharenites with a lesser proportion of quartz arenites. Sandstones from the Chia Zinnar section are unusual in that they are arkosic in composition (Table 1, Figure 4). Monocrystalline quartz is the most common component; most grains are angular to subangular and have uniform extinction. Inclusions in quartz grains include vacuoles, apatite, zircon, rutile, tourmaline and iron oxides (Figures 5 and 6). Polycrystalline quartz is a minor component. Fresh and altered orthoclase feldspars occur, in addition to a few plagioclase and microcline grains (Figures 5a, 5b, 5c and 6a, 6b, 6c). Plagioclase grains, with typical polysynthetic twinning, are subangular and slightly altered to clay minerals (Figure 6c). Chert and carbonate grains are the main lithic fragments with minor occurrences of plutonic and mudstone grains (Figures 5d, 5e and 6b, 6d). Micas also are commonly present

Table 2. Major element data (wt%) for sandstones from the Khabour Formation. Data from the Akkas-1 and -3 wells were original documented in Al Juboury et al. (2021).

Section	SampleNo	SiO_2	Al_2O_3	Fe_2O_3	MgO	CaO	Na_2O	K_2O	TiO_2	MnO	P_2O_5
Akkas-1 well	AK1_KH_S1	71.28	1.89	3.49	3.32	7.57	0.23	0.52	0.14	0.17	0.08
	AK1_KH_S2	72.88	12.49	4.31	0.86	0.95	1.34	3.27	0.42	0.03	0.09
	AK1_KH_S3	73.55	12.51	3.80	0.80	0.74	1.65	3.39	0.35	0.04	0.08
	AK1_KH_S4	75.72	10.77	3.31	0.64	1.08	1.86	2.92	0.55	0.04	0.08
	AK1_KH_S5	74.69	11.75	3.43	0.83	0.66	2.21	2.89	0.59	0.03	0.08
	AK1_KH_S6	65.96	14.66	5.75	1.91	2.01	1.63	2.53	0.79	0.11	0.09
	AK1_KH_S7	67.31	13.60	5.80	1.88	1.98	1.51	2.43	0.70	0.10	0.08
	AK1_KH_S8	74.51	11.85	3.27	0.90	0.76	2.74	2.02	0.71	0.03	0.08
	AK1_KH_S9	73.80	10.30	3.20	0.77	2.32	2.12	1.88	0.65	0.11	0.08
	AK1_KH_S10	72.27	9.20	2.83	0.54	4.98	2.36	1.48	0.45	0.15	0.08
	AK1_KH_S11	57.51	18.82	6.20	1.67	2.86	1.68	3.40	0.95	0.15	0.12
Ave		70.82	12.59	4.19	1.08	1.83	1.91	2.62	0.61	0.08	0.08
Max		75.72	18.82	6.20	1.91	4.98	2.74	3.40	0.95	0.15	0.12
Min		57.51	9.20	2.83	0.54	0.74	1.34	1.48	0.35	0.03	0.08
Akkas-3 well	AK3_KH_S1	65.76	16.23	5.76	1.82	0.43	2.38	3.08	0.88	0.03	0.22
	AK3_KH_S5	76.79	9.59	4.26	0.91	0.69	3.11	0.51	1.01	0.03	0.09
	AK3_KH_S8	77.24	9.88	3.59	0.80	0.79	3.26	0.66	0.69	0.03	0.09
	AK3_KH_S11	65.15	19.08	3.10	1.14	0.21	2.48	4.19	0.89	0.02	0.08
	AK3_KH_S18	61.88	21.17	2.76	1.26	0.25	2.16	4.96	1.02	0.02	0.05
	AK3_KH_S25	70.93	12.91	5.05	1.17	1.38	2.71	1.40	0.61	0.08	0.09
	AK3_KH_S27	73.17	12.99	4.15	1.01	0.41	1.81	2.97	0.44	0.03	0.07
	AK3_KH_S29	52.13	23.73	4.56	2.01	0.24	0.01	6.04	2.03	0.03	0.10
	AK3_KH_S30	74.79	11.66	2.33	0.68	1.33	2.89	1.85	0.73	0.04	0.10
	AK3_KH_S38	69.62	13.81	3.32	1.05	1.26	0.01	2.57	0.85	0.03	0.53
Ave		68.74	15.10	3.88	1.18	0.69	2.08	2.82	0.91	0.03	0.14
Max		77.24	23.73	5.76	2.01	1.38	3.26	6.04	2.03	0.08	0.53
Min		52.13	9.59	2.33	0.68	0.21	0.01	0.51	0.69	0.02	0.05
Khabour	KHB_KH_S1	92.22	2.14	3.09	0.31	0.41	0.11	0.36	0.24	0.12	0.18
	KHB_KH_S2	88.76	5.05	4.06	0.32	0.42	0.12	0.31	0.22	0.12	0.20
	KHB_KH_S3	81.05	7.84	5.78	0.70	0.46	0.66	1.92	0.72	0.28	0.24
	KHB_KH_S4	86.03	6.11	3.78	0.90	0.24	0.12	1.56	0.51	0.01	0.11
	KHB_KH_S5	69.18	17.18	4.79	1.12	0.47	0.16	5.97	0.93	0.09	0.23
	KHB_KH_S6	73.39	13.75	4.80	0.84	0.50	0.15	5.04	0.77	0.10	0.27
	KHB_KH_S7	71.22	14.61	8.90	0.67	0.32	0.19	2.72	0.88	0.01	0.09
	KHB_KH_S8	71.65	12.36	8.45	0.59	0.31	0.18	2.59	0.81	0.01	0.09
	KHB_KH_S9	75.09	7.32	9.02	0.65	0.42	0.15	2.77	0.81	0.01	0.09
	KHB_KH_S10	70.87	12.09	8.33	0.81	0.39	0.19	2.87	0.82	0.02	0.09
	KHB_KH_S11	77.74	5.88	9.92	0.87	0.40	0.16	3.43	0.81	0.01	0.09
	KHB_KH_S12	76.76	4.83	8.70	0.68	0.29	0.17	2.72	0.98	0.01	0.08
	KHB_KH_S13	75.63	8.36	2.16	0.69	0.12	0.16	8.13	1.30	0.01	0.06
	KHB_KH_S14	74.92	4.65	5.40	1.41	0.24	0.41	2.13	1.26	0.02	0.17
	KHB_KH_S15	75.52	21.94	1.90	0.91	0.16	0.15	7.50	1.34	0.01	0.07
	KHB_KH_S16	77.22	3.68	5.80	0.94	0.28	0.14	4.71	1.21	0.01	0.09
	KHB_KH_S17	76.63	4.61	6.36	0.88	0.29	0.12	4.52	1.28	0.01	0.08
	KHB_KH_S18	81.43	4.09	5.25	0.74	0.28	0.14	3.02	0.88	0.01	0.09
	KHB_KH_S19	74.22	6.81	8.10	0.77	0.52	0.13	3.62	0.91	0.01	0.07
Ave		77.34	8.59	6.03	0.77	0.34	0.19	3.46	0.87	0.04	0.12

Table 2. (Continued).

Max		92.22	21.94	9.92	1.41	0.52	0.66	8.13	1.36	0.28	0.27
Min		69.18	2.14	1.90	0.31	0.12	0.11	0.31	0.22	0.01	0.06
Chalki Nasara	CH-N -1	88.41	5.46	1.71	0.34	0.09	0.30	1.85	0.68	0.03	0.05
	CH-N -3	82.42	7.83	3.18	0.63	0.16	1.32	2.07	0.59	0.06	0.08
	CH-N -7	89.57	5.20	1.52	0.30	0.10	0.84	1.71	0.27	0.03	0.05
	CH-N -12	81.47	9.22	2.88	0.69	0.16	0.98	2.68	0.44	0.01	0.06
	CH-N -19	85.05	6.94	2.48	0.53	0.33	0.65	1.91	0.42	0.14	0.06
	CH-N -27	85.11	7.03	2.30	0.37	0.11	0.38	3.13	0.26	0.01	0.08
	CH-N -35	94.47	1.53	1.87	0.12	0.09	0.03	0.64	0.44	0.20	0.05
	CH-N -39	84.66	6.81	3.11	0.51	0.25	0.78	2.05	0.38	0.10	0.15
	CH-N -44	93.54	3.04	1.67	0.26	0.10	0.11	1.09	0.26	0.04	0.06
	CH-N -47	94.38	2.21	1.44	0.22	0.18	0.09	0.58	0.29	0.01	0.13
	CH-N -49	92.00	1.84	1.73	0.66	0.34	0.36	0.67	0.65	0.05	1.01
	CH-N -55	90.15	5.01	3.56	0.55	9.12	0.79	0.70	0.35	0.09	0.39
	CH-N -61	93.11	2.03	1.30	0.47	0.78	0.05	0.84	0.26	0.07	0.26
	CH-N -64	84.67	6.18	3.17	0.63	0.24	0.81	1.03	0.38	0.24	0.12
	CH-N -68	90.25	1.80	2.00	0.23	5.92	0.15	0.30	0.64	0.06	0.57
	CH-N -75	89.65	3.59	3.24	0.55	0.42	0.05	0.62	0.31	0.01	0.29
	CH-N -79	95.10	2.01	1.20	0.34	0.18	0.04	0.71	0.21	0.04	0.21
Ave		89.05	4.57	2.25	0.43	1.09	0.45	1.32	0.40	0.07	0.21
Max		95.10	9.22	3.56	0.69	9.12	0.98	3.13	0.68	0.24	1.01
Min		82.42	1.53	1.20	0.12	0.09	0.04	0.30	0.21	0.01	0.05
Ora	2	94.77	1.77	1.68	0.26	0.13	0.11	0.27	0.33	0.01	0.10
	9	94.91	1.80	1.30	0.25	21.60	0.15	0.55	0.34	0.09	0.15
	10	89.47	4.44	2.03	0.35	0.30	0.26	1.74	0.40	0.02	0.22
	20	84.01	6.84	3.31	0.46	0.16	0.69	2.19	0.48	0.24	0.07
	22	86.44	5.31	2.63	0.54	0.71	0.26	1.68	0.33	0.01	0.50
	24	84.16	5.77	4.11	0.67	0.61	0.16	1.23	0.47	0.07	0.44
	31	89.54	3.59	2.62	0.33	0.23	0.18	1.12	0.37	0.08	0.16
	34	87.66	4.42	2.27	0.42	0.88	0.21	1.40	0.34	0.05	0.63
	49	84.71	6.80	2.88	0.56	0.23	0.63	1.97	0.33	0.01	0.11
	52	94.16	2.00	1.37	0.19	0.08	0.05	0.39	0.21	0.01	0.06
Ave		88.98	4.27	2.42	0.40	2.49	0.27	1.25	0.36	0.05	0.24
Max		94.91	6.84	4.11	0.67	21.60	0.69	2.19	0.48	0.24	0.63
Min		84.01	1.77	1.30	0.19	0.08	0.05	0.27	0.21	0.01	0.06

and represented mostly by plutonic muscovite (Figures 5c, 5d and 6e). Zircon, rutile and, rarely, tourmaline are the dominate heavy minerals (Figures 5f, 5c). Siliciclastic matrix commonly exists and consists of dark clay material, altered feldspar, and lithic fragments, with some aphanitic material. Three types of cement were observed; ferruginous cement, calcite cement, and rare silica cement (Figures 5 and 6). The composition of the representative XRD samples (Figure 7) indicates that these sandstones are composed of quartz, mica, and feldspars (labradorite, orthoclase, microcline, anorthite, and albite) in addition to clay minerals, mainly chlorite with small amounts of kaolinite and illite. The sandstones are typically very fine- to fine-grained, moderately sorted and texturally immature (Figures 5d and 6f).

A SEM was used to study both the framework grains and matrix; images are presented in Figure 8. The SEM revealed that small quartz overgrowths on detrital grains are more common than the petrographic study suggested (Figure 8A). Feldspar grains usually have pitted surfaces and are typically undergoing alteration into kaolinite and illite (Figure 8B). Mica flakes with degraded rims and crenulated habits are also common (Figure 8C). The images also illustrate the broad distribution of carbonates as both scattered lithic fragments and as cement filling pores and fractures (Figure 8D). The images show that microporosity exists as fractures and vugs that are either open or partly filled (Figures 8B, 8C). Regarding the clay component, the SEM analysis reveals the common occurrence of disk-shaped chlorite (Figure 8D) and indicates that illite and kaolinite are more common than the XRD results suggest. Illite is typically present as flakes and fibers (Figure 8E). Hexagonal plates and booklets of kaolinite are partially degraded (Figure 8F).

Table 3. Trace element data (ppm) for sandstones from the Khabour Formation (note that Co, Sc, and Pb are not annlysed for the Chalki Nasara and Ora sections). Data from the Akkas-1 and -3 wells were original documented in Al Juboury et al. (2021).

Section	Sample number	Ni	Co	Cr	V	Sc	Cu	Zn	Pb	Sr	Rb	Ba	Zr	Nb	Hf	Th	La	U
Akkas-1 well	AK1_KH_S1	3.43	0.21	8.81	13.11	1.12	5.12	223.5	12.42	70.42	113.8	569.7	140.14	18.6	4.23	2.44	37.4	1.21
	AK1_KH_S2	18.70	6.00	35.10	53.00	7.10	17.20	65.10	36.80	193.30	97.10	689.80	179.00	8.90	5.00	7.40	22.90	1.50
	AK1_KH_S3	17.90	5.80	34.70	53.70	7.00	12.10	63.50	53.80	217.90	100.70	700.30	111.40	7.50	3.00	6.50	25.90	1.70
	AK1_KH_S4	15.30	5.00	29.40	41.90	6.20	21.70	134.50	35.40	203.20	81.10	653.60	509.40	10.30	12.00	12.50	27.40	2.70
	AK1_KH_S5	16.20	4.60	38.10	47.40	7.20	15.10	53.30	29.10	203.40	83.70	654.30	415.10	11.30	10.00	11.30	24.70	2.60
	AK1_KH_S6	35.00	14.60	70.50	96.40	12.20	27.00	90.40	23.10	166.10	99.90	448.00	223.40	17.40	6.00	11.80	36.90	2.70
	AK1_KH_S7	28.30	10.30	55.20	76.90	9.70	19.20	86.50	20.20	175.30	69.50	472.60	511.80	15.40	13.00	12.90	29.80	3.30
	AK1_KH_S8	15.20	4.30	45.90	63.00	7.20	13.70	79.60	268.50	325.60	47.70	358.10	488.60	9.60	9.00	12.10	24.90	2.90
	AK1_KH_S9	13.50	7.80	29.60	38.50	4.40	32.60	108.50	17.40	249.00	134.90	765.20	240.60	21.00	6.00	17.30	55.50	3.90
	AK1_KH_S10	29.00	9.20	79.90	66.80	11.90	30.70	99.30	12.40	70.40	15.70	91.20	140.10	2.70	13.00	2.40	10.60	1.10
	AK1_KH_S11	39.90	15.30	104.80	129.10	20.00	27.10	80.70	36.90	193.40	96.70	689.90	178.80	8.90	9.00	7.40	22.90	1.50
Akkas-3 well	AK3_KH_S1	38.76	12.52	80.89	110.38	14.52	20.01	94.33	17.54	155.88	113.82	569.69	205.92	18.57	0.28	11.28	37.37	2.35
	AK3_KH_S5	13.78	4.10	51.86	83.96	7.07	7.17	40.64	15.36	163.97	18.86	427.24	835.20	20.38	0.26	19.80	43.74	3.54
	AK3_KH_S8	10.85	2.97	38.95	64.69	6.33	7.12	28.58	12.66	156.88	24.84	312.60	504.54	14.27	0.19	13.24	31.12	2.25
	AK3_KH_S11	13.96	4.92	61.72	93.72	12.89	10.10	25.41	11.55	118.56	143.11	772.50	398.11	19.08	0.29	12.56	32.03	2.68
	AK3_KH_S18	17.23	8.05	82.37	123.35	17.15	9.96	35.24	12.61	152.43	164.91	1283.88	431.59	21.46	0.39	16.30	50.52	3.19
	AK3_KH_S25	22.72	7.95	50.07	72.76	9.45	12.16	61.47	17.01	168.14	54.67	390.52	256.28	12.47	0.18	9.23	27.50	1.62
	AK3_KH_S27	19.46	6.73	40.18	62.66	7.78	10.83	175.68	27.94	185.18	92.77	597.48	202.61	9.42	0.34	7.98	25.81	1.75
	AK3_KH_S29	39.75	35.37	226.12	287.81	30.08	16.16	59.21	36.56	282.09	234.24	1430.57	582.94	45.84	3.42	35.90	144.13	7.78
	AK3_KH_S30	12.21	6.08	51.73	77.24	9.89	11.30	32.02	30.03	163.75	68.15	1263.49	471.42	15.18	0.37	14.24	41.76	2.69
	AK3_KH_S38	18.70	8.66	72.72	93.86	13.30	9.70	53.45	15.88	230.52	93.96	728.65	440.63	18.75	0.98	19.01	52.22	3.52
Khabour	KHB_KH_S1	17.70	8.10	12.20	13.20	4.20	18.40	309.50	38.80	49.00	12.00	122.20	155.50	4.20	5.00	19.80	34.90	1.00
	KHB_KH_S2	17.50	8.50	39.30	44.40	9.40	19.90	41.40	20.60	70.30	59.20	353.70	558.10	11.90	15.00	18.70	40.30	2.50
	KHB_KH_S3	18.40	2.10	29.70	36.50	5.60	5.00	12.80	9.40	25.70	45.40	148.80	321.90	8.00	9.00	16.70	34.90	1.50
	KHB_KH_S4	23.40	9.30	76.90	95.30	16.80	10.80	38.60	16.50	107.10	161.50	734.60	294.90	17.50	8.00	14.90	46.00	2.70
	KHB_KH_S5	21.00	7.10	49.50	67.90	12.50	19.80	40.30	22.40	100.10	117.80	705.00	396.10	13.30	11.00	15.10	38.00	2.70
	KHB_KH_S6	42.20	12.10	66.90	101.30	13.40	5.90	40.50	8.50	72.80	83.20	220.00	539.50	17.90	14.00	15.50	38.40	3.50
	KHB_KH_S7	22.30	2.70	89.20	120.40	16.50	10.50	11.30	19.80	81.70	168.90	521.70	550.90	43.20	16.00	22.30	74.40	15.00
	KHB_KH_S8	40.70	8.60	136.40	125.90	18.10	18.90	106.30	19.20	95.80	80.70	315.20	370.90	28.00	10.00	22.00	64.30	3.90
	KHB_KH_S9	32.70	2.10	107.80	314.30	18.10	154.50	14.50	18.90	66.00	182.90	483.70	626.70	35.90	11.00	28.80	71.00	25.30
	KHB_KH_S10	36.90	11.20	104.20	125.60	19.00	23.10	79.70	33.90	188.60	95.70	686.90	174.60	7.90	12.00	8.40	21.40	1.30
	KHB_KH_S11	16.70	8.40	132.20	125.20	9.20	15.90	376.40	37.50	77.10	53.00	143.20	172.50	6.20	10.00	19.60	35.90	1.00
	KHB_KH_S12	20.50	9.50	89.30	56.20	9.90	32.10	87.40	30.60	90.30	58.20	398.70	602.10	10.90	9.00	20.70	38.30	2.20
	KHB_KH_S13	29.40	9.10	87.70	136.50	8.80	20.80	66.80	19.40	75.70	49.40	248.80	451.90	9.60	13.00	21.70	38.90	1.90
	KHB_KH_S14	31.40	10.30	86.50	129.30	16.20	19.80	39.20	18.50	102.10	71.50	634.50	284.50	12.50	14.00	13.90	36.00	2.20

Table 3. (Continued).

	KHB_KH_S15	30.00	9.10	69.50	117.90	12.50	17.80	50.30	19.40	102.10	88.80	717.00	388.10	13.10	10.00	17.10	38.30	2.50
	KHB_KH_S16	53.20	12.40	70.10	121.30	12.40	13.20	45.80	12.40	72.80	85.20	230.00	619.50	17.90	10.00	15.50	38.40	3.50
	KHB_KH_S17	40.30	4.70	89.20	130.40	18.50	13.50	41.30	17.80	87.70	98.90	521.40	540.30	33.20	12.00	22.30	64.40	5.00
	KHB_KH_S18	23.70	9.50	136.30	129.90	17.10	17.90	106.20	16.20	75.70	87.70	415.20	390.90	18.90	11.00	19.00	63.30	3.90
	KHB_KH_S19	34.70	2.70	127.60	294.80	19.10	54.50	84.50	16.90	66.60	82.90	483.40	636.70	25.90	8.00	28.10	69.00	5.10
Chalki Nasara	CH-N -1	7.00		25.00	30.00		5.00	17.00		36.00	55.00	257.00	506.00	14.00	18.00	14.00	38.00	4.00
	CH-N -3	12.00		26.00	36.00		10.00	24.00		54.00	58.00	413.00	622.00	13.00	27.00	16.00	44.00	4.00
	CH-N -7	5.00		14.00	15.00		2.00	19.00		39.00	46.00	290.00	165.00	6.00	22.00	4.00	20.00	2.00
	CH-N -12	10.00		32.00	47.00		1.00	18.00		56.00	77.00	386.00	247.00	10.00	26.00	8.00	32.00	2.00
	CH-N -19	10.00		16.00	32.00		2.00	13.00		36.00	59.00	310.00	290.00	9.00	14.00	8.00	35.00	3.00
	CH-N -27	10.00		22.00	22.00		19.00	16.00		76.00	81.00	593.00	153.00	6.00	13.00	5.00	18.00	1.00
	CH-N -35	6.00		39.00	20.00		4.00	14.00		27.00	22.00	165.00	275.00	8.00	23.00	10.00	31.00	2.00
	CH-N -39	14.00		56.00	33.00		18.00	148.00		60.00	57.00	488.00	206.00	9.00	14.00	7.00	37.00	2.00
	CH-N -44	6.00		19.00	16.00		6.00	85.00		30.00	35.00	202.00	150.00	6.00	27.00	9.00	28.00	2.00
	CH-N -47	8.00		79.00	17.00		11.00	40.00		42.00	18.00	107.00	142.00	6.00	28.00	20.00	48.00	1.00
	CH-N -49	20.00		47.00	45.00		28.00	60.00		104.00	50.00	233.00	896.00	14.00	16.00	31.00	79.00	7.00
	CH-N -55	35.00		20.00	45.00		35.00	127.00		600.00	27.00	2769.00	180.00	6.00	17.00	8.00	108.00	10.00
	CH-N -61	23.00		30.00	33.00		23.00	74.00		271.00	36.00	283.00	468.00	13.00	16.00	26.00	85.00	6.00
	CH-N -64	16.00		24.00	28.00		14.00	56.00		44.00	36.00	407.00	183.00	9.00	6.00	10.00	35.00	2.00
	CH-N -68	25.00		24.00	50.00		91.00	714.00		485.00	11.00	206.00	2611.00	39.00	22.00	11.00	162.00	10.00
	CH-N -75	15.00		53.00	18.00		9.00	36.00		49.00	19.00	116.00	175.00	6.00	21.00	11.00	33.00	1.00
	CH-N -79	20.00		35.00	34.00		38.00	41.00		75.00	78.00	1610.00	345.00	9.00	15.00	11.00	22.00	4.00
Ora	2	10.00		18.00	12.00		5.00	224.00		22.00	10.00	25.00	130.00	6.00	17.00	16.00	45.00	1.00
	9	29.00		19.00	50.00		21.00	20.00		1015.00	20.00	258.00	172.00	5.00	5.00	9.00	168.00	11.00
	10	7.00		15.00	25.00		4.00	15.00		44.00	49.00	305.00	281.00	7.00	18.00	10.00	34.00	1.00
	20	14.00		25.00	31.00		29.00	54.00		55.00	59.00	498.00	298.00	9.00	29.00	11.00	30.00	4.00
	22	15.00		13.00	21.00		11.00	20.00		67.00	43.00	299.00	185.00	7.00	17.00	10.00	30.00	2.00
	24	19.00		22.00	30.00		17.00	274.00		36.00	36.00	208.00	216.00	9.00	14.00	11.00	29.00	2.00
	31	39.00		13.00	24.00		23.00	33.00		36.00	32.00	195.00	192.00	8.00	22.00	12.00	32.00	1.00
	34	18.00		18.00	27.00		21.00	173.00		67.00	38.00	299.00	184.00	8.00	17.00	15.00	37.00	2.00
	49	15.00		24.00	25.00		22.00	36.00		50.00	53.00	369.00	156.00	8.00	25.00	6.00	22.00	3.00
	52	10.00		16.00	13.00		4.00	17.00		17.00	12.00	48.00	83.00	6.00	14.00	11.00	30.00	1.00

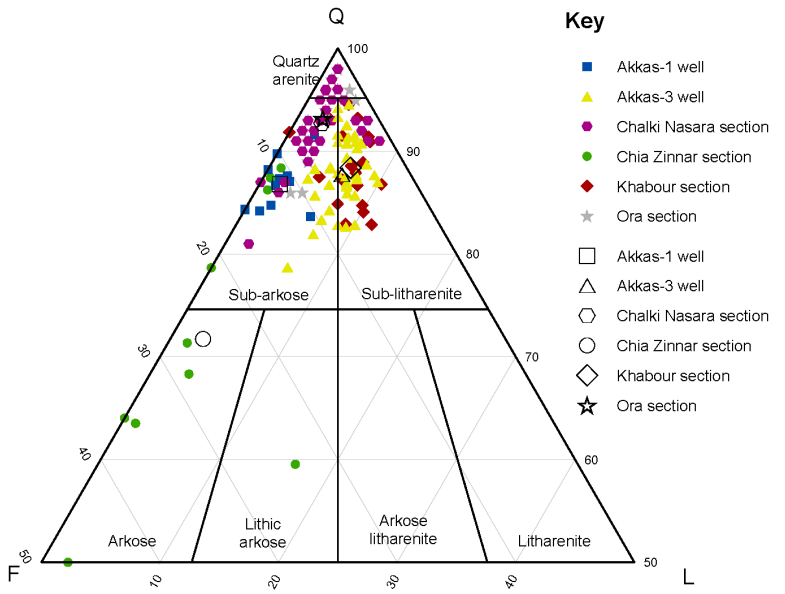

Figure 4. QFL plot showing the composition of sandstones from the Cambro–Ordovician Khabour Formation in the Akkas-1 well compared to the same formation in the Akkas-3 well, and the Khabour, Chalki Nasara, Ora and Chia Zinnar sections. Mean compositions in each section are indicated by the open symbols. The classification scheme is from Folk (1974).

4.2. Geochemistry

Major and trace element abundances from 67 samples from both outcrop and the subsurface are presented in Tables 2 and 3. Various elemental ratios sensitive to paleoweathering, provenance, and tectonic setting are listed in Table 4. From the major elemental data, SiO_2 average values in the subsurface Akkas-1 and Akkas-3 wells are 70.82% and 68.74%, which are less than those of surface Khabour, Chaki Nasara, and Ora sections that are 77.34%, 89.05%, and 88.98% respectively (Table 2). Conversely, Al_2O_3 average values are higher in the subsurface sections (12.59% and 15.10% for the Akkas-1 and Akkas-3 wells respectively) compared to those for the Khabour, Chalki Nasara, and Ora sections (8.59%, 4.50% and 4.27% respectively). The average values of MgO, K_2O, and Na_2O also are higher in subsurface sections as compared to the surface outcrop sections (Table 2). The average values of Fe_2O_3, CaO, TiO_2, MnO, and P_2O_5 show no distinctive variation between the subsurface and surface sections (Table 2).

Trace element data are presented in Table 3. Some ratios of these elements can be used for the discrimination of various paleoclimatic, paleoweathering, and provenance conditions. These are presented in Table 4.

5. Discussion

5.1. Provenance

The ratio of Al_2O_3/TiO_2 can be used to determine provenance/source area composition because these oxides are immobile during weathering, transportation, and diagenesis. According to Hayashi et al. (1997), the Al_2O_3/TiO_2 ratio for mafic rocks ranges from 3 to 8, 8 to 21 for intermediate, and 21 to 70 for felsic igneous rocks. The average value of Al_2O3/TiO_2 is 21.59 for the sandstones of the Akkas-1 well, 17.90 for the Akkas-3 well, and 10.75 for the Khabour, 12.41 for the Chalki Nasara, and 11.72 for the Ora outcrop sections (Table 4). These average values are within the range of intermediate and felsic sources. This is supported by the petrographic results of the studied sandstones that indicate they are composed of quartz (both mono- and-polycrystalline) and feldspars, such as plagioclase, orthoclase, and microcline, in addition to mica (both biotite and muscovite) and lithic grains that are dominated by metamorphic, andesitic igneous and chert fragments.

Another ratio used to determine the provenance of clastic rocks is TiO_2/Zr. If its value is more than 195, it refers to mafic igneous rock sources, where the value is 55 to 195, it may indicate igneous rocks of intermediate type,

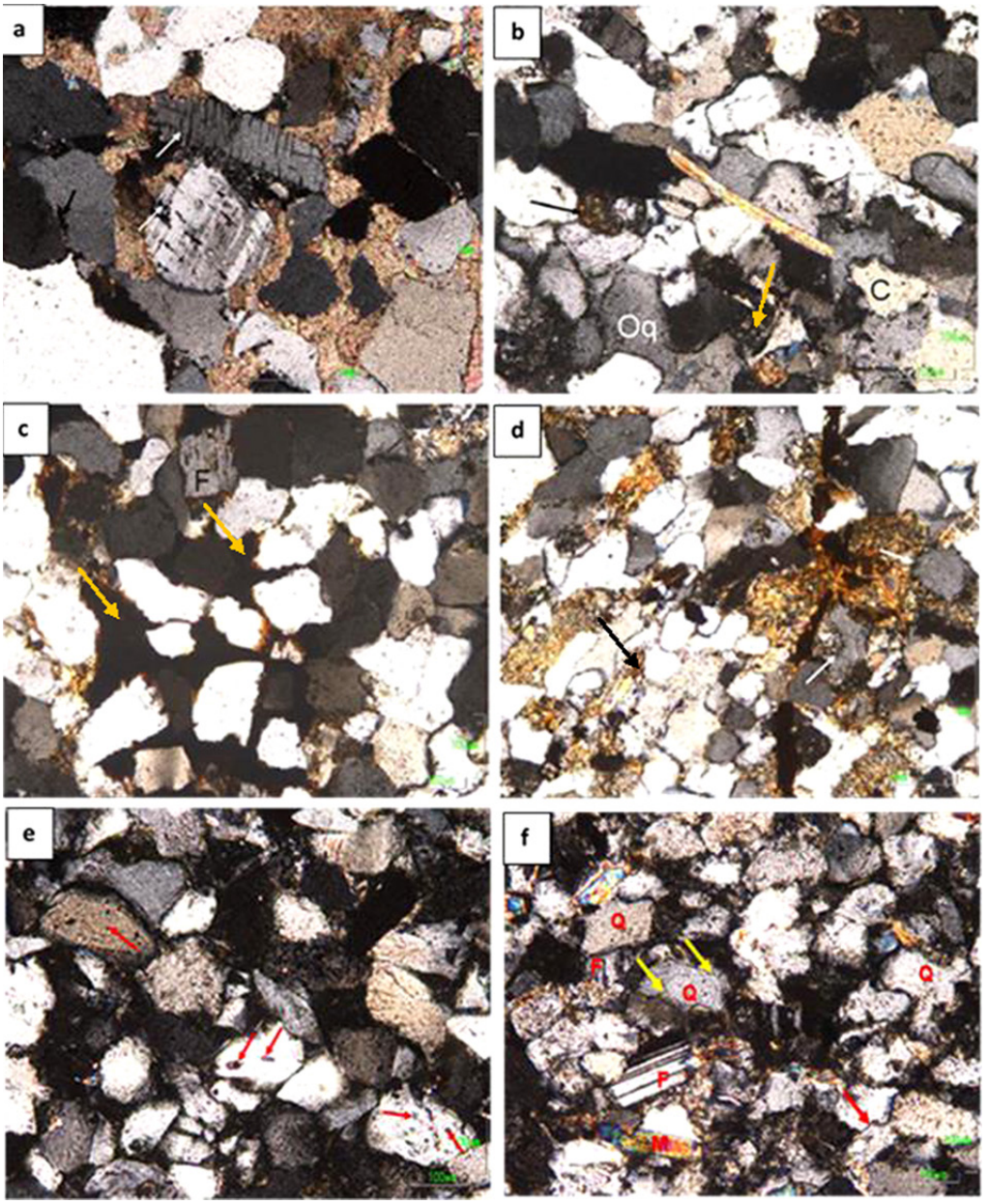

Figure 5. Photomicrographs showing petrographic components of the studied sandstones (a) Subarkose sandstone showing feldspars and quartz in pervasive carbonate cement. Note the corroded grains of feldspar with intracrystalline porosity (white arrows) and corrosion and pores also on quartz grains margins (black arrow). XPL, sample AK1_KH_S1. (b) Subarkose showing pervasive ferruginous cements (Fc), note the corroded margins of quartz and feldspar (F) grains. XPL, sample KHB_KH_S1. (c) Subarkose showing monocrystalline quartz (Q) with secondary silica overgrowths (yellow arrows). Quartz is enriched with inclusions of vacuoles, spherulitic zircon and iron oxides. Note the feldspar (F), some altered, altered mica (M) with micropores and sutured contacts (red arrow). XPL, sample AK3_KH_S39. (d) Calcite-cemented subarkose showing fresh uncompacted mica, a quartz overgrowth (Oq) and calcite (C); Fe-dolomite (arrow) also exists. XPL, sample AK1_KH_S9. (e) Sublitharenite showing corrosion at quartz grain margins that may lead to secondary porosity development (arrows), note the embayment in a quartz grain after carbonate cement replacement. XPL, sample KHB_KH_S14. (f) Subarkose showing common inclusions in monocrystalline quartz (arrows), including enlongated and spherulitic zircon, vacuoles and iron oxides. XPL, sample AK3_KH_S14.

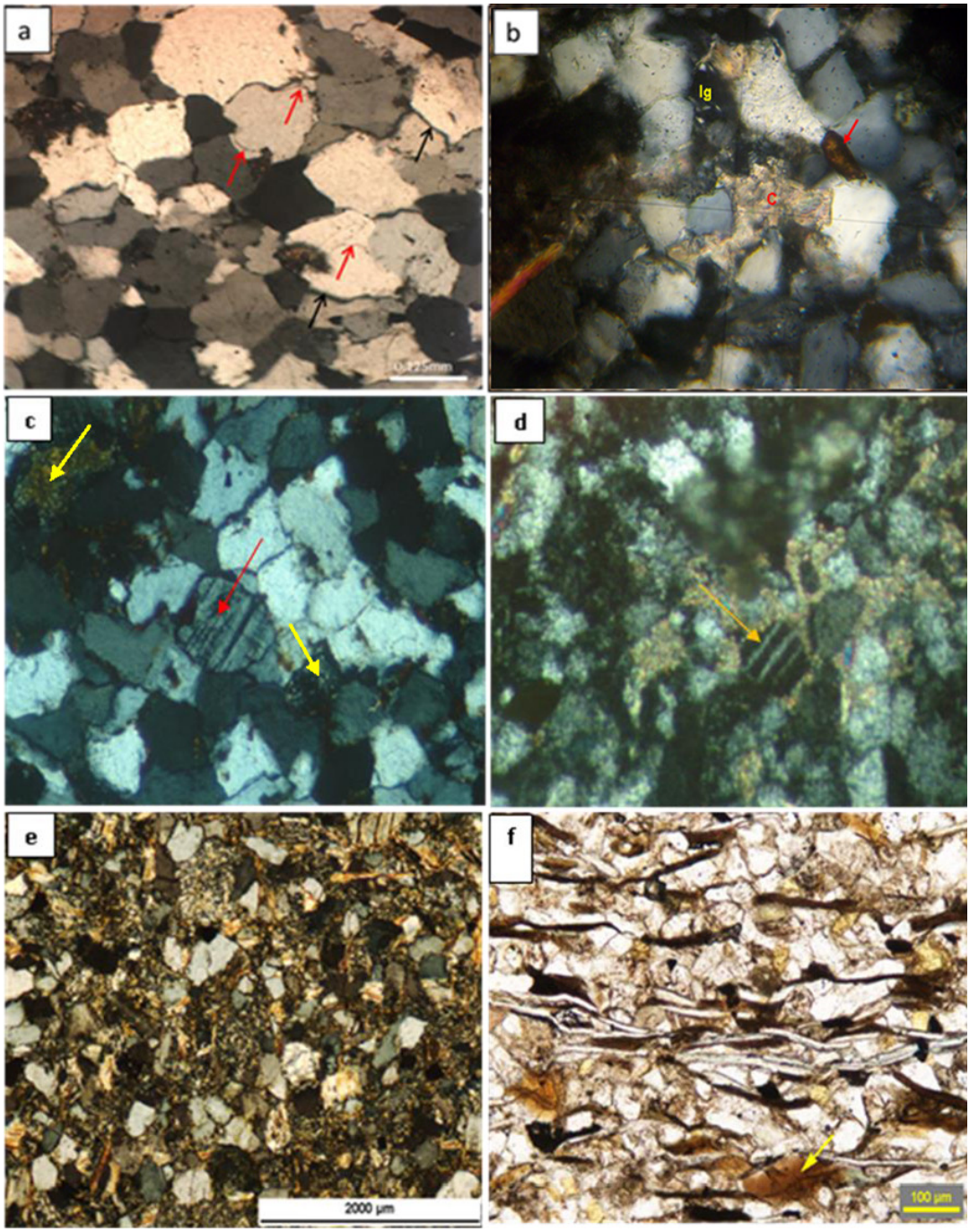

Figure 6. Photomicrographs showing petrographic components of the studied sandstones (a) Syntaxial quartz (red arrows) showing subrounded grain, fractured and altered feldspar and ferrugineous cement (black arrows). XPL, sample CH-N 39. (b) Subarkose sandstone showing a subrounded, fractured and altered feldspar (red arrow). XPL, sample KH.-N 39. (c) Subarkose sandstone showing fresh feldspar plagioclase (arrow) surrounded by authigenic clay. XPL, sample CH-N 3. (d) Immature sublitharenite displaying low mechanical compaction between detrital grains. XPL, sample Ora 5. (e) Subarkose containing common muscovite and brown biotite flakes that accentuate the sample's planar laminar fabric. A few biotite flakes are oriented along the plane of the photograph (arrow). PPL, Chia Zinnar section, sample B6228. (f) Fine-grained subarkose comprising mostly subrounded to rounded quartz and ?feldspar grains. XPL, sample CH-N 26.

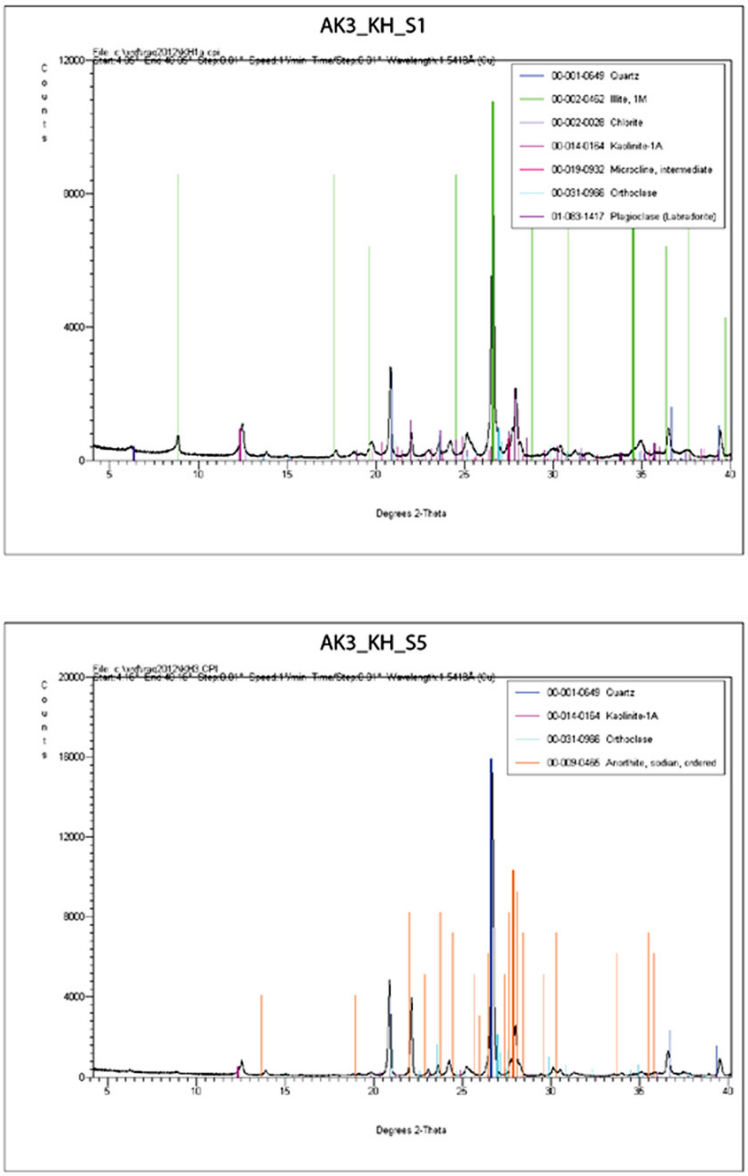

Figure 7. X-ray diffractograms for selected bulk sandstone samples illustrating the main mineralogical components.

whereas values of <55 may indicate felsic igneous rocks (McLennan et al. 1993; Basu et al. 2017). The average value of this ratio is 25.6 for the sandstones of the Akkas-1 well, 22.97 for the Akkas-3 well, and 23.41 for the Khabour, 14.12 for the Chalki Nasara and 19.93 for the Ora outcrop sections (Table 4). These average values are within the range of felsic sources. In the present study, the binary plot of TiO_2 versus Zr reveals that most samples were derived from felsic igneous rock sources. This result also is supported by the TiO_2 versus Zr plot of McLennan et al. (1993), (Figure 9).

Trace element ratios such as La/Sc, Th/Sc, La/Co, Cr/Th, and Th/Co are commonly used to differentiate between the igneous, mafic, and felsic rock sources (Wronkiewicz and Condie, 1990; Cox et al., 1995; Cullers, 1995; Cullers, 2000). In the present study (Table 4), these ratios support derivation from felsic rock sources.

The La/Th versus Hf plot is another useful parameter for providing the composition of source areas (Floyd and Leveridge, 1987). The average value of La/Th is 2.97 for the sandstones of the Akkas-1 well, 2.94 for the Akkas-3 well, and 2.46 for the Khabour, 4.64 for the Chalki Nasara and

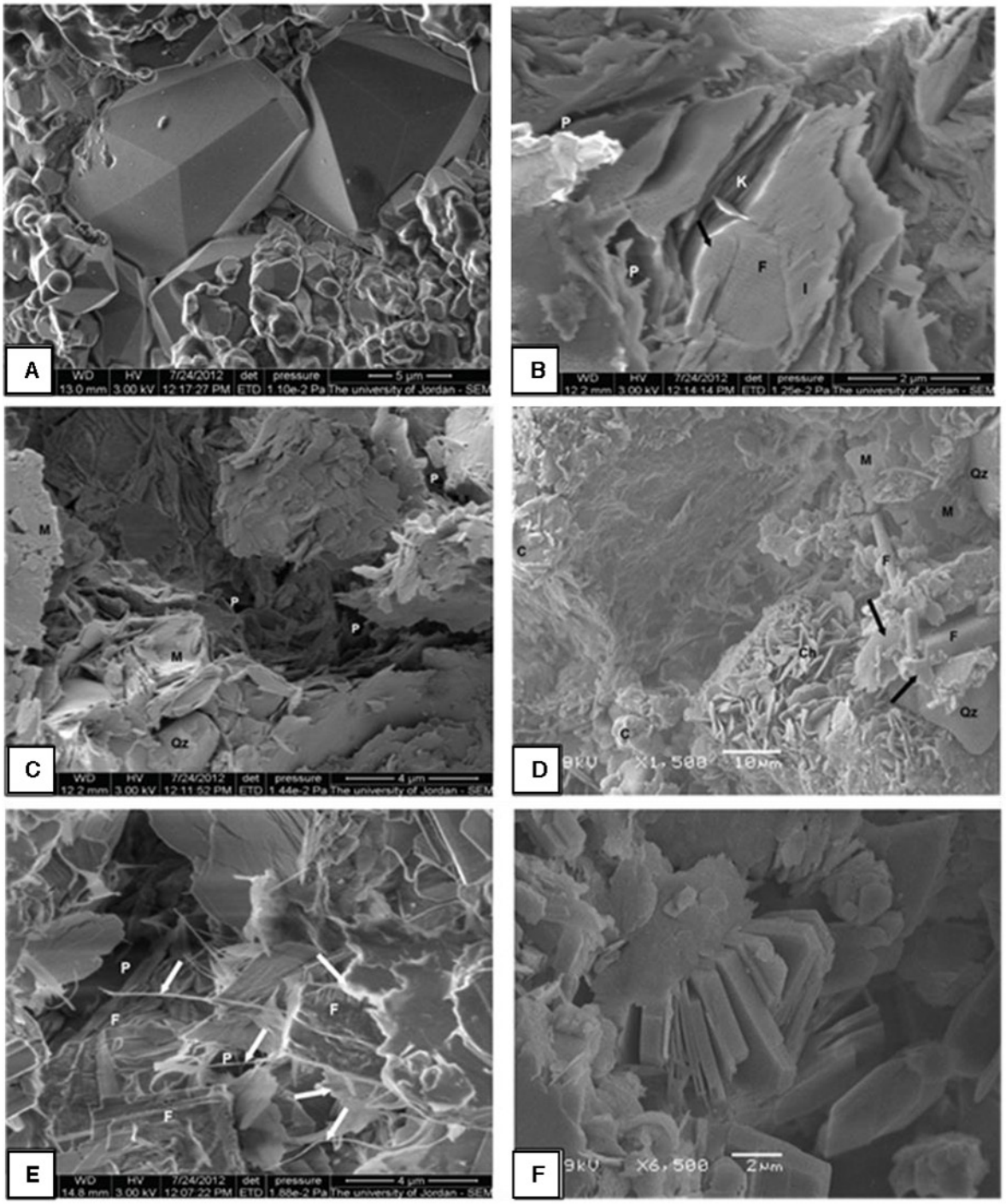

Figure 8. SEM images showing sandstones from the Khabour Formation in the Akkas-3 well. A: Various stages of secondary authigenic quartz formation with overgrowths filling pore spaces in sample AK3_KH_S17. B: Degraded feldspar grain (F) showing alteration to illite fibers (I), note presence of kaolinite plates (K) and common pores (P) sample AK3_KH_S16. C: Crenulated mica flakes (M), quartz (Qz) and microporosity (P), sample AK3_KH_S15. D: Carbonate lithic grains(C), feldspar (F), quartz (Qz), mica flakes (M), with illite flakes (arrows) and common chlorite disc-shaped crystals (Ch), sample AK3_KH_S8. E: Illite fibres (arrows) growing from precursor feldspar grains (F), note presence of microporosity (P) in sample AK3_KH_S32. F: Hexagonal Kaolinite booklets infilling pores, sample AK3_KH_S36.

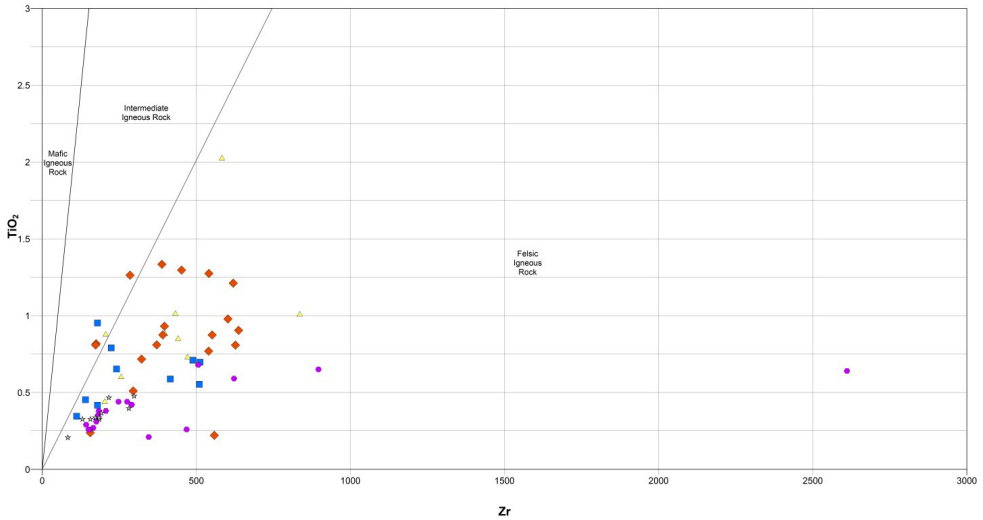

Figure 9. TiO_2 versus Zr bivariate provenance diagram for sandstone samples from the Khabour Formation (after McLennan et al. 1993).

4.48 for the Ora outcrop sections (Table 4). These average values are higher than those recorded from Post Archean Australian Shale (PAAS), (2.61) and Upper Continental Crust (UCC), (2.8) (Taylor and McLennan, 1985) (Table 4). Plotting La/Th versus Hf (Figure 10) shows that most of the sandstone samples are close to the field of felsic igneous rock sources. Accordingly, the plot of TiO_2 versus Ni (Figure 11) also shows that most of the studied Khabour Formation sandstones fall near the acidic and magmatic rock source fields.

The major element data also provides important information on the nature of the source area. Sandstones with more than 77% SiO_2 are derived from quartz-rich crystalline provenance (Zaid and Al Ghatani, 2015). In the present study, the average of SiO_2 in the studied sandstone reaches (79%, Table 2) reflecting the high percentage of quartz (average 89%, Table 1). Monocrystalline quartz is the dominant framework grain component and is mainly of plutonic origin while polycrystalline quartz is composed of a stretched metamorphic type (Folk, 1974). Lithic grain compositions indicate of component of sediment sourcing from sedimentary and plutonic (granitic) rocks. Some textural features including fine- to medium-grain size and good sorting with predominately subrounded to rounded grain shapes, along with low feldspar (average 4.3%) and rock fragment (average 6.9%) contents (Table 1) may imply a cratonic source region subjected to long moderate chemical weathering in a warm and dry climate (e.g., Amireh, 1991; Al Habri and Khan, 2008). Double or triple coaxial crystal overgrowths on quartz grains (Figures 5b, 5f; 6a; 8A) indicate multiple phases of recycling of this cratonic source likely in a passive continental margin setting. The presence of illite and kaolinite (Figure 8), and the absence/scarcity of smectite also suggest their derivation from the weathering of felsic (granitic) rock sources. Acid igneous sources are also indicated by the common presence of the heavy minerals zircon, rutile, anatase, and tourmaline in the studied sandstones. The CIA and CIW values (average 73, Table 4) of the Khabour Formation sandstone reflect a low-relief source area with low-moderate weathering and dominating humid climatic conditions. Monocrystalline quartz with undulatory extinction is the common framework grain with common inclusions such as; vacuoles, zircon, rutile, muscovite, apatite, and iron oxides. Varying proportions of sedimentary, metasedimentary and volcanic lithics are also occur in the Khabour Formation sandstones (Figures 4 and 5). Sedimentary lithics are dominantly chert. Plagioclase, orthoclase, and twinned microcline are the common feldspar types in the studied sandstones. Mica is commonly observed in the form of mica laths and biotite. Quartz types with undulosity extinction along with common inclusions may indicate derivation from a dominantly plutonic (granitic) provenance in a setting of continental crust and continental arc (Basu et al., 1975).

5.2. Paleoweathering

Chemical weathering is strongly affected by the mineralogical and geochemical composition of siliciclastic rocks (Nesbitt and Young, 1982; Johnsson et al., 1988) which, in turn, is strongly influenced by various factors such as provenance, tectonic uplift and climatic conditions of the source area (Wronkiewicz and Condie, 1987). In the present study, weathering indices such as the Chemical Index of Alteration (CIA), Index of Compositional

Table 4. Elemental ratios sensitive to paleoweathering, provenance, and tectonic setting conditions of the study samples.

Section	**Sample No.**	**Al_2O_3/TiO_2**	**La/Th**	**Rb/Sr**	**TiO_2/Zr**	**CIA**	**ICV**	**K_2O/Na_2O**	**SiO_2/Al_2O_3**	**$logK_2O/Na_2O$**
	AK1_KH_S1	13.5	15.3	1.62	9.99	18.51	0.63	2.26	37.7	0.35
Akkas-1 well	AK1_KH_S2	29.88	3.09	0.50	23.35	72.95	0.82	2.44	5.84	0.39
	AK1_KH_S3	36.16	3.98	0.46	31.06	71.16	0.80	2.06	5.88	0.31
	AK1_KH_S4	19.44	2.19	0.40	10.88	69.14	0.87	1.57	7.03	0.20
	AK1_KH_S5	19.95	2.19	0.41	14.19	69.58	0.85	1.31	6.36	0.12
	AK1_KH_S6	18.53	3.13	0.60	35.41	77.74	0.87	1.55	4.50	0.19
	AK1_KH_S7	19.48	2.31	0.40	13.64	77.37	0.92	1.61	4.95	0.21
	AK1_KH_S8	16.67	2.06	0.15	14.55	71.16	0.82	0.74	6.29	-0.13
	AK1_KH_S9	15.75	3.21	0.54	27.18	71.83	0.85	0.89	7.17	-0.05
	AK1_KH_S10	20.26	4.42	0.22	32.41	70.09	0.86	0.63	7.86	-0.20
	AK1_KH_S11	19.75	3.09	0.50	53.30	78.56	0.75	2.03	3.06	0.31
Ave		21.59	2.97	0.52	25.60	72.95	0.84	1.55	8.78	0.15
Max		36.16	4.42	1.62	53.30	78.56	0.92	2.44	37.7	0.39
Min		15.75	2.06	0.15	10.88	69.14	0.75	0.63	4.50	-0.20
Akkas-3 well	AK3_KH_S1	18.40	3.31	0.73	42.83	74.69	0.86	1.30	4.05	0.11
	AK3_KH_S5	9.47	2.21	0.12	12.12	72.36	1.03	0.16	8.01	-0.79
	AK3_KH_S8	14.38	2.35	0.16	13.62	71.31	0.92	0.20	7.82	-0.69
	AK3_KH_S11	21.54	2.55	1.21	22.24	73.97	0.62	1.69	3.41	0.23
	AK3_KH_S18	20.81	3.10	1.08	23.57	74.74	0.58	2.30	2.92	0.36
	AK3_KH_S25	21.32	2.98	0.33	23.63	75.67	0.86	0.52	5.49	-0.29
	AK3_KH_S27	29.29	3.23	0.50	21.89	73.01	0.80	1.64	5.63	0.22
	AK3_KH_S29	11.69	4.01	0.83	34.81	79.68	0.62	603.83	2.20	2.78
	AK3_KH_S30	15.90	2.93	0.42	15.56	70.91	0.73	0.64	6.41	-0.19
	AK3_KH_S38	16.17	2.75	0.41	19.38	84.20	0.57	204.50	5.04	2.31
Ave		17.90	2.94	0.56	22.97	75.05	0.76	81.67	5.09	0.40
Max		29.29	4.01	1.21	42.83	84.20	1.03	603.83	8.01	2.78
Min		9.47	2.21	0.16	12.12	70.91	0.57	0.16	2.20	-0.79
Khabour	KHB_KH_S1	8.95	1.76	0.24	15.37	81.73	1.98	3.30	43.09	0.52
	KHB_KH_S2	22.75	2.16	0.84	3.98	92.03	1.02	2.60	17.58	0.41
	KHB_KH_S3	10.92	2.09	1.77	22.31	75.17	1.28	2.91	10.34	0.46
	KHB_KH_S4	11.96	3.09	1.51	17.33	78.39	1.13	13.02	14.08	1.11
	KHB_KH_S5	18.43	2.52	1.18	23.53	73.70	0.76	37.28	4.03	1.57
	KHB_KH_S6	17.86	2.48	1.14	14.27	72.56	0.85	33.62	5.34	1.53
	KHB_KH_S7	16.70	3.34	2.07	15.88	83.36	0.92	14.33	4.87	1.16
	KHB_KH_S8	15.24	2.92	0.84	21.87	81.67	1.02	14.39	5.80	1.16
	KHB_KH_S9	9.05	2.47	2.77	12.91	71.47	1.83	18.45	10.26	1.27
	KHB_KH_S10	14.78	2.55	0.51	46.85	79.78	1.08	15.11	5.86	1.18
	KHB_KH_S11	7.26	1.83	0.69	46.96	62.04	2.59	21.45	13.22	1.33
	KHB_KH_S12	4.93	1.85	0.64	16.26	62.52	2.75	16.02	15.89	1.20
	KHB_KH_S13	6.45	1.79	0.65	28.70	50.20	1.49	50.81	9.05	1.71
	KHB_KH_S14	3.68	2.59	0.70	44.43	64.66	2.29	5.20	16.11	0.72
	KHB_KH_S15	16.43	2.24	0.87	34.40	74.15	0.54	49.99	3.44	1.70
	KHB_KH_S16	3.04	2.48	1.17	19.56	43.11	3.48	33.66	20.98	1.53
	KHB_KH_S17	3.62	2.89	1.13	23.60	49.80	2.86	37.69	16.62	1.58
	KHB_KH_S18	4.67	3.33	1.16	22.38	56.37	2.45	21.59	19.91	1.33
	KHB_KH_S19	7.52	2.46	1.24	14.21	64.43	1.99	27.87	10.90	1.45
Ave		10.75	2.46	1.11	23.41	69.32	1.70	22.06	13.01	1.20
Max		22.75	3.34	2.77	46.96	92.03	3.48	50.81	43.09	1.71
Min		3.04	1.76	0.24	3.98	43.11	0.54	2.60	4.03	0.41

Table 4. (Continued).

Chalki Nasara	CH-N -1	8.03	2.71	1.53	13.44	71.70	0.90	6.17	16.19	0.79
	CH-N -3	13.27	2.75	1.07	9.49	69.65	1.01	1.57	10.53	0.20
	CH-N -7	19.26	5.00	1.18	16.36	66.98	0.90	2.04	17.23	0.31
	CH-N -12	20.95	4.00	1.38	17.81	71.50	0.83	2.73	8.84	0.44
	CH-N -19	16.52	4.38	1.64	14.48	72.97	0.88	2.94	12.26	0.47
	CH-N -27	27.04	3.60	1.07	16.99	66.66	0.92	8.24	12.11	0.92
	CH-N -35	3.48	3.10	0.81	16.00	69.51	2.16	21.33	61.75	1.33
	CH-N -39	17.92	5.29	0.95	18.45	70.55	1.02	2.63	12.43	0.42
	CH-N -44	11.69	3.11	1.17	17.33	71.70	1.13	9.91	30.77	1.00
	CH-N -47	7.62	2.40	0.43	20.42	76.69	1.19	6.44	42.71	0.81
	CH-N -49	2.83	2.55	0.48	7.25	64.11	2.24	1.86	50.00	0.27
	CH-N -55	14.31	13.50	0.05	19.44	75.34	1.24	0.89	17.99	-0.05
	CH-N -61	7.81	3.27	0.13	5.56	69.21	1.48	16.80	45.87	1.23
	CH-N -64	16.26	3.50	0.82	20.77	76.93	1.02	1.27	13.70	0.10
	CH-N -68	2.81	14.73	0.02	2.45	76.49	1.94	2.00	50.14	0.30
	CH-N -75	11.58	3.00	0.39	17.71	84.14	1.33	12.40	24.97	1.09
	CH-N -79	9.57	2.00	1.04	6.09	72.76	1.26	17.75	47.31	1.25
Ave		12.41	4.64	0.83	14.12	72.17	1.26	6.88	27.92	0.64
Max		27.04	14.73	1.64	20.77	84.14	2.24	21.33	61.75	1.25
Min		2.81	2.00	0.02	2.45	64.11	0.83	0.89	8.84	-0.05
Ora	2	5.36	2.81	0.45	25.38	82.30	1.50	2.45	53.54	0.39
	9	5.29	18.67	0.02	19.77	62.44	1.70	3.67	52.73	0.56
	10	11.10	3.40	1.11	14.23	68.93	1.08	6.69	20.15	0.83
	20	14.25	2.73	1.07	16.11	70.29	1.08	3.17	12.28	0.50
	22	16.09	3.00	0.64	17.84	73.16	1.03	6.46	16.28	0.81
	24	12.28	2.64	1.00	21.76	80.49	1.16	7.69	14.59	0.89
	31	9.70	2.67	0.89	19.27	73.40	1.31	6.22	24.94	0.79
	34	13.00	2.47	0.57	18.48	73.15	1.06	6.67	19.83	0.82
	49	20.61	3.67	1.06	21.15	72.26	0.94	3.13	12.46	0.50
	52	9.52	2.73	0.71	25.30	81.95	1.11	7.80	47.08	0.89
Ave		11.72	4.48	0.75	19.93	73.84	1.20	5.39	27.38	0.69
Max		20.61	18.67	1.11	25.38	82.30	1.70		53.54	0.89
Min		5.29	2.47	0.02	14.23	62.44	0.94		12.28	0.39

Variability (ICV), Chemical Index of Weathering (CIW), and the Th/U ratio are employed to determine the degree of source area weathering.

The Chemical Index of Alteration (CIA; Nesbitt and Young, 1982) is commonly used as an index to evaluate the degree of weathering and palaeoclimatic fluctuations. It is expressed as CIA = $[Al_2O_3/(Al_2O_3 + CaO^* + Na_2O + K_2O)] \times 100$, where Al_2O_3, CaO, Na_2O, and K_2O are in molar proportion and CaO^* is the amount of CaO incorporated in the silicate fractions of the rock. Thus, samples with a high content of CaO related to diagenetic cement must be corrected using the equation of Fedo et al. (1995): $CaO^* = CaO - (10.3 \times P_2O_5)$. If the obtained CaO is less than Na_2O, no correction is needed; if it is more than Na_2O, we consider CaO equal to Na_2O (McLennan et al., 1993). Generally, CIA values ranging from 50 to 70 imply slight weathering, from 70 to 80 imply moderate weathering, and above 80 imply intense weathering conditions (Nesbitt and Young, 1982, 1989). The average value of CIA is ~ 73 for sandstones from the Akkas-1 well, ~ 75 for the Akkas-3 well, ~ 69 for the Khabour section, ~ 72 for the Chalki Nasara section and ~ 73 for the Ora section (Table 4). These average values reveal moderate chemical weathering in the source area and suggest a warm and humid climate. Plotting CIA versus Al_2O_3 values is useful for evaluating the degree of chemical weathering (Obasi and Madukwe, 2016). In this plot, the majority of the studied samples lie in the 60 to 80 field, whilst others lie within the 80 to 100 field; this suggests mainly moderate and, to a lesser extent, intense weathering conditions (Figure 12).

The Index of Compositional Variability (ICV; Cox et al., 1995) is also used to identify the compositional maturity of clastic rocks. Some minerals like feldspar, amphibole, and pyroxene have ICV values larger than 1, these are considered diagenetically resistant minerals, while

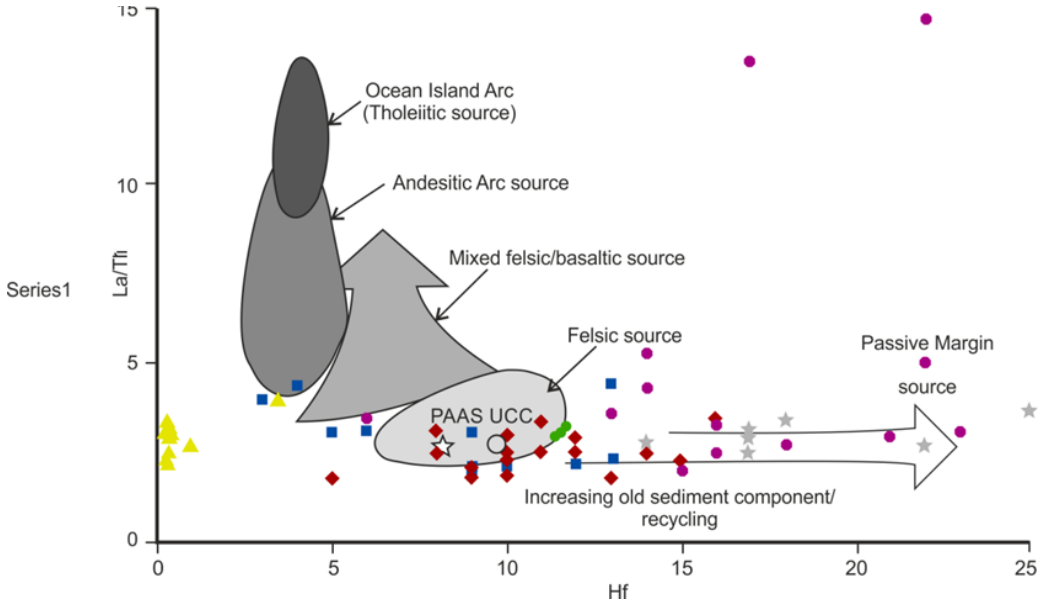

Figure 10. La/Th vs. Hf diagram for the sandstones of the Khabour Formation (after Floyd and Leveridge, 1987).

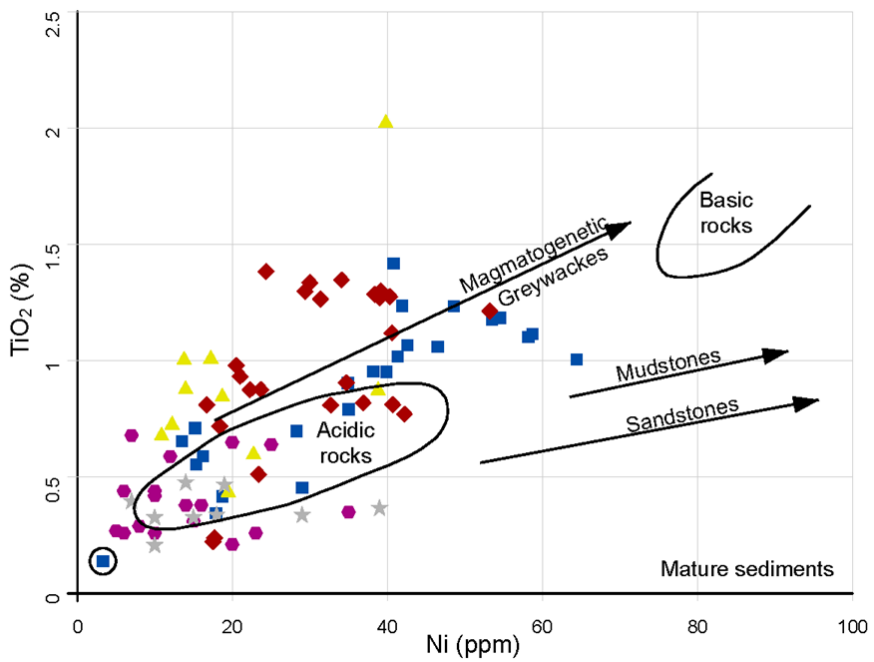

Figure 11. TiO_2 vs Ni plot (Floyd et al., 1989) indicating that the majority of the Khabour Formation sandstones plot near the acidic and magmatic source. Sample AK1_KH_S1 is highlighted by a black circle.

alteration products such as kaolinite, illite, and muscovite have ICV values less than 1 (Cox et al., 1995; Cullers and Podkovyrov, 2000; Mahdi et al., 2021). Therefore, sediments with low ICV values typically imply multiple phases of recycling and/or strong weathering. The average value of ICV is 0.84 for the sandstones of the Akkas-1 well, 0.76 for the Akkas-3 well, and 1.70 for the Khabour, 1.26 for the Chalki Nasara and 1.20 for the Ora outcrop sections (Table 4). The average of these results is higher than 1 for the outcrop samples and less than 1 for the well samples. This would suggest that the well samples have been more deeply buried, and subject to burial diagenesis, than the outcrop samples.

The A–CN–K ternary diagram is used to determine the weathering trend of elements (Nesbitt and Young, 1982). Plotting data on this diagram shows a variable degree of weathering; Khabour and Ora samples lying parallel to the A–K line close to the illite point have experienced moderate weathering intensities, whereas other sections display low to moderate degree of weathering (Figure 13).

The Th/U ratio signifies the intensity of chemical weathering in rock source areas (McLennan et al., 1995). Clastic sedimentary rocks that form due to chemical weathering of the upper continental crust are characterized by a Th/U ratio ≥ 4, whereas Th/U ratios < 4 have been related to the derivation of sediments from depleted mantle sources (Roddaz et al., 2006). The average ratio of Th/U is ~4 for the sandstones of the Akkas-1 well, 5.17 for the Akkas-3 well, 7.45 for Khabour section, 4.92 for the Chalki Nasara section and 7.26 for the Ora section (Table 4). Plotting data on the McLennan et al. (1993) diagram shows that weathering increased at the source area (Figure 14). This indicates that sediments were derived from a source area with a moderate degree of weathering. The values of CIA and ICV with the A-CN-K plot revealed moderate weathering in humid climatic conditions at the source areas.

5.3. Paleoclimate

The plot of SiO_2 versus $Al_2O_3+K_2O+Na_2O$ in Figure 15 shows that the samples plot in both the humid and arid climatic zones. The obtained results correlate well with the petrographic data which show high amounts of quartz as a result of humid climate conditions especially in the surface sections (Ora and Khabour sections, see Figure 16 and Table 1), while lower quartz contents are recorded for the subsurface sections (Akkas-1 and Akkas-3) where arid climatic conditions dominated. This climatic situation is also supported by palynoflora studies by Baban and Lawa (2016) and Al Juboury et al. (2020) for the Khabour Formation in northern Iraq, implying a moist warm climate. However, based on a palynological study of the Khabour Formation at its type locality (Al Juboury et al., 2020), variation from humid to dry and warm conditions was recorded. A warm, semiarid to arid palaeoclimate was also reported from the clay mineral distributions. The presence of kaolinite indicates a prevailing humid climate and illite dry conditions, whilst the presence of chlorite as a detrital clay, which does not typically survive in cool moist environments, is a good indicator of cool/dry climates (Chamley, 1989). These three minerals are recorded in the studied sandstone of the Khabour Formation (Figure 7).

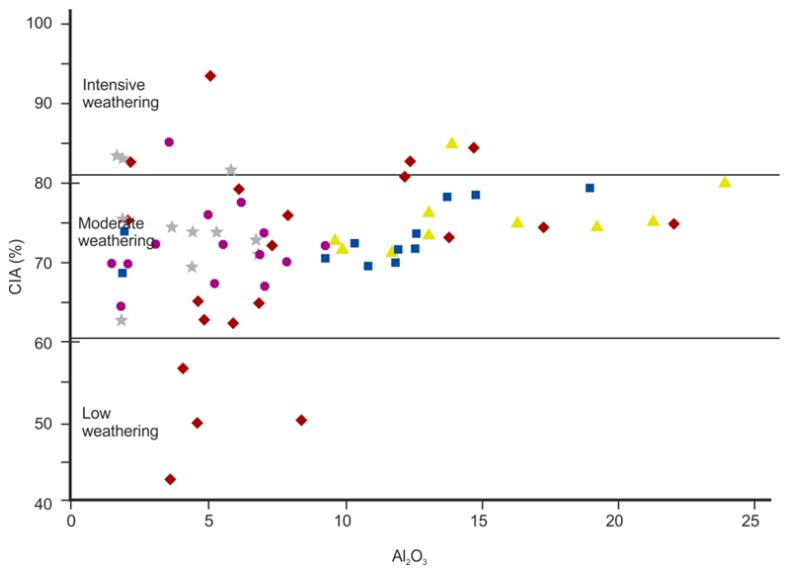

Figure 12. Chemical index of alteration (CIA) versus Al_2O_3 crossplot of the studied samples (after Obasi and Madukwe, 2016).

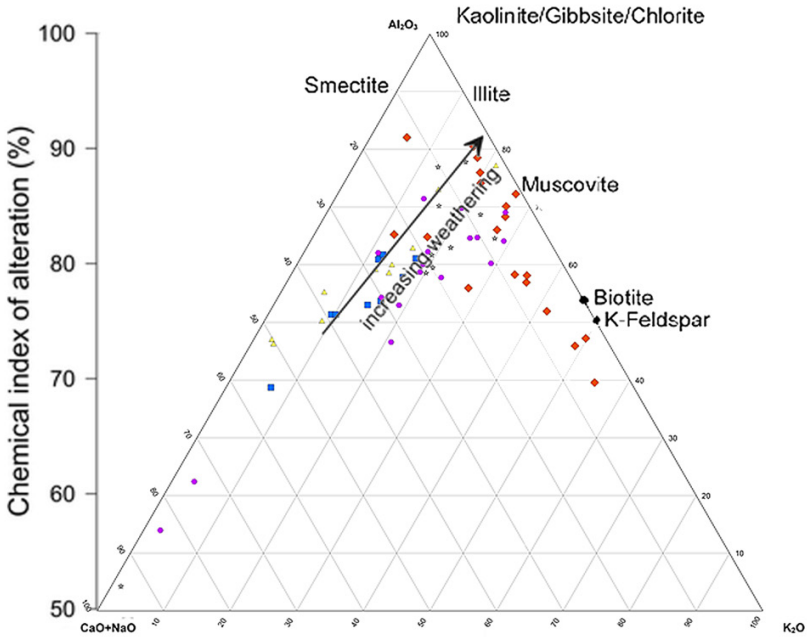

Figure 13. The Al_2O_3– CaO + Na_2O–K_2O (A–CN–K) ternary diagram of the studied samples (after Nesbitt and Young, 1982).

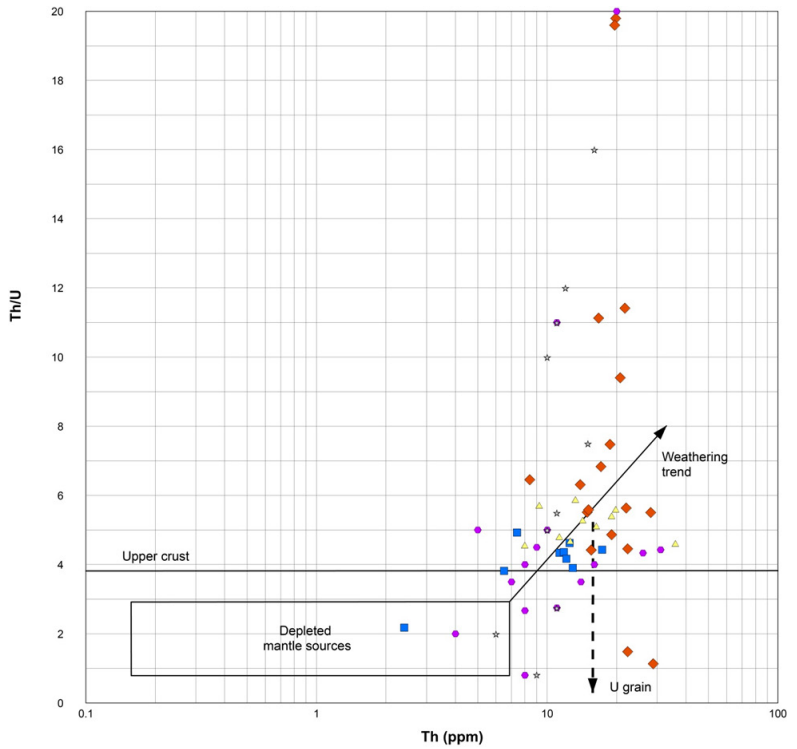

Figure 14. Th/U versus Th diagram of the studied samples showing weathering trends (after McLennan et al., 1993).

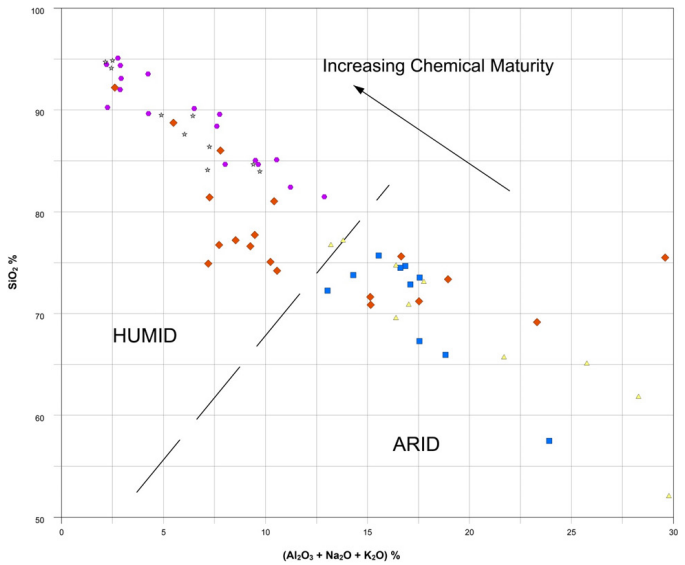

Figure 15. Bivariate plot of SiO_2 versus Al_2O_3+ K_2O + Na_2O of the sandstone of the Khabour Formation (after Suttner and Dutta, 1986).

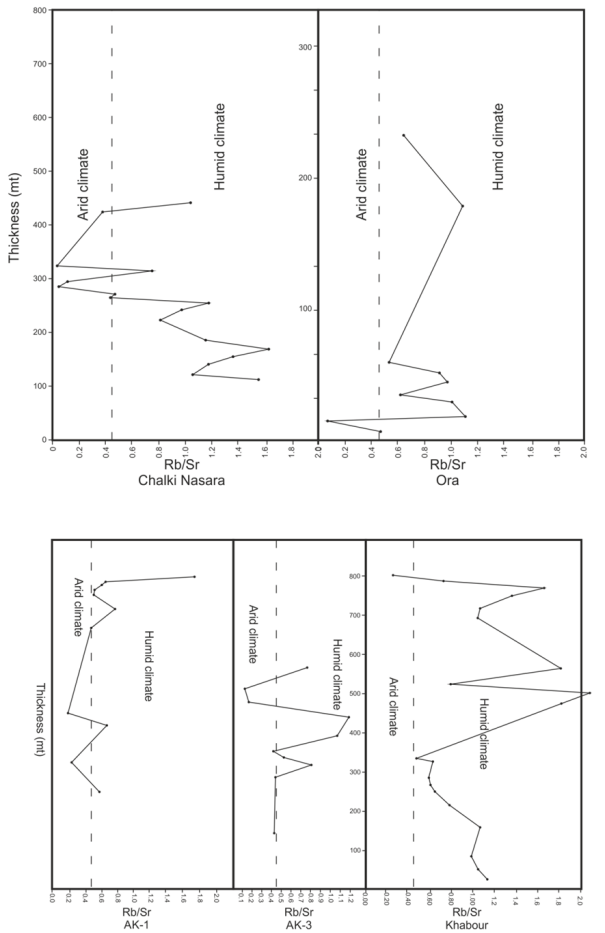

Figure 16. Rb/Sr ratio versus thickness of the studied outcrop and well sections (the threshold discrimination boundary is at 0.45, Zou et al., 2021).

Petrographic data show that quartz grains, feldspars and rock fragments types may suggest moderate chemical weathering in a warm humid climate at the source area (Pettijohn et al., 1987).

The Rb/Sr ratio is considered a key paleoclimate indicator (Cao et al., 2012; Al Haj et al., 2019; Cusack et al., 2020). These two elements behave differentially in the weathering process. Rb is sTable relative to Sr, therefore, it is likely to resist weathering and stay in parent rocks compared to Sr. In humid climates where the weathering is intense, the Rb is more likely to be leached out and Rb/Sr ratio increased, while in arid climate Sr is only weathered and hence Rb/Sr ratio decreased (Jinhua et al., 2018). The Rb/Sr value of 0.45 is suggested as a threshold value to discriminate between arid and humid climates (Zou et al., 2021).

In the current study, the plot of Rb/Sr (Figure 16) versus sample height in each section revealed that there is a variation in the trend of arid and humid conditions up section in the Khabour succession. The fact that subsurface samples mostly fall in the arid field and surface sections mostly in the humid field may result from surficial weathering at outcrop.

5.4. Tectonic setting

The chemical composition of sedimentary rocks can also give some clues about the tectonic setting of their depositional basin (e.g., Bhatia, 1983; Bhatia and Crook, 1986; Roser and Korsch, 1986, 1988; Verma and Armstrong Altrin, 2013). Discrimination function-based diagrams were introduced by Verma and Armstrong Altrin (2013) to utilize oxide concentrations of major elements for tectonic setting determination of siliciclastic sediments. They developed two sets of diagrams, optimized for either low silica (35% to 63% SiO_2) or high silica rocks (63% to 95% SiO_2), which were successfully tested on Neogene–Quaternary as well as Precambrian sediments.

The SiO_2 contents of the sandstones analysed in this study are more than 63% (Table 2), which classifies them as high-silica clastics. Most of the sandstone samples fall into the rift field, which coincides with the passive margin/intracratonic setting (Figure 17). The Khabour Formation was deposited in a passive margin setting (Sharland et al., 2001; Jassim and Buday, 2006). Additionally, many workers use combinations of the geochemical and petrographical data to assign passive margin/intracratonic settings for different Paleozoic sandstones of the Arabian Platform (Hussain, 2001; Al Harbi and Khan, 2005; Wanas and Abdel Maguid, 2006; Al Harbi and Khan, 2008, 2011; Bassis, 2017). In addition to the passive margin source, however, there is a possible presence of older collisional sources from active regions probably represented by the basement rocks of Neoproterozoic age of the Arabian Shield and/or syn-rift toward NE Iraq.

The Khabour Formation sandstones plot in the recycled orogen and continental block provenances with sTable craton sources and with uplifting in the basement complexes (Figure 18). Craton interior field represents the mature sandstones derived from relatively low-lying igneous and metamorphic sources (Dickinson et al. 1983).

The Khabour sandstones in northern Iraq represent the shelf deposition of the northern Gondwana passive margin without being influenced by rifting and magmatism caused by the opening of Paleo-Tethys (Omer et al., 2021).

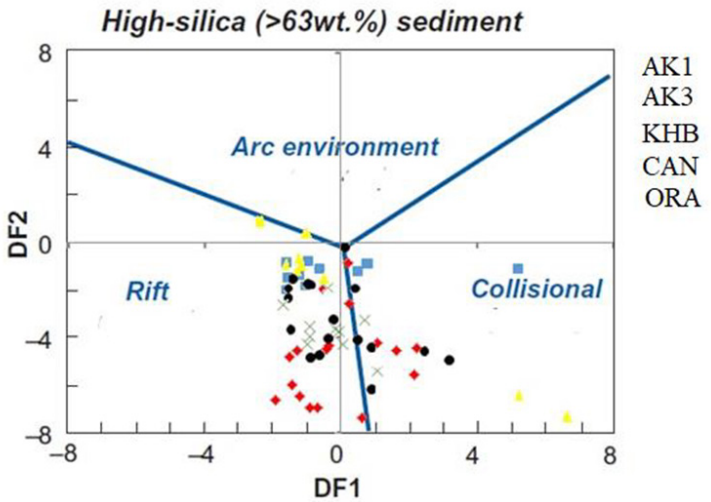

Figure 17. Tectonic setting discrimination diagram after Verma and Armstrong-Altrin (2013) illustrating an active rift setting for the source of majority of the Khabour Formation sandstones.

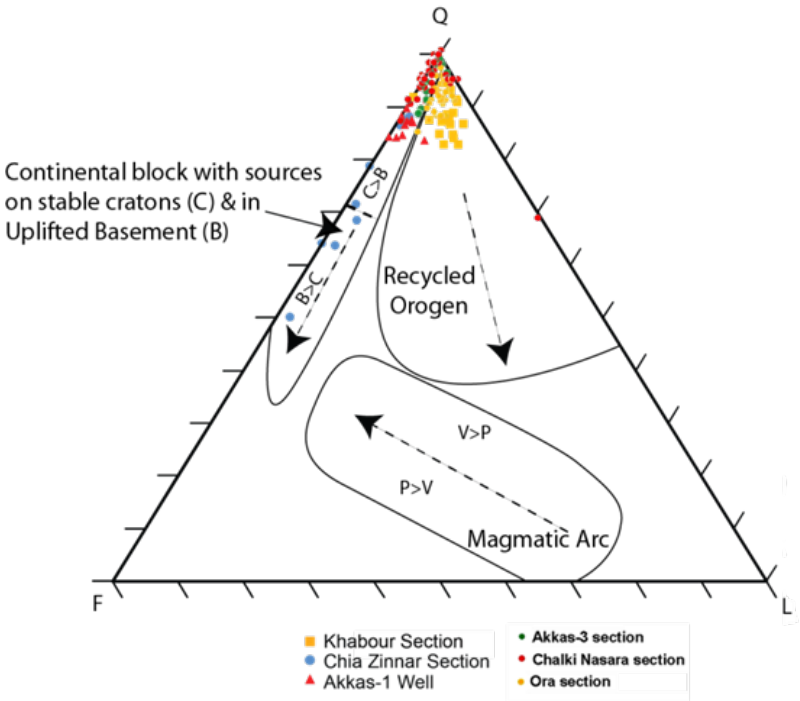

Figure 18. Petrographic data of the Khabour Formation plotted on the QFL discrimination diagram of Dickinson and Suczek (1979), for definitions and overlapping on some of points in the diagram see data in Table 1.

6. Conclusions

The oldest known Paleozoic sandstones from both subsurface and surface sections in Iraq are represented by the Khabour Formation. These have been subjected to petrographic, mineralogical and geochemical investigations in this study. This reveals that these sandstones are mostly subarkoses and sublitharenites with few quartz arenites types. Petrographic components suggest a granitic source with minor input from metamorphosed sediments, most likely from exposed basement of the Arabian shield. Chemical Index of Alteration and Index of Chemical Variability values in conjunction with A-CN-K trends, and Th/U versus Th relationships suggest moderate weathering in humid climatic conditions in the source area. Clay minerals distribution and paleoclimate geochemical proxies suggest both humid and dry prevailing conditions. Up section trends in Rb/Sr values suggest that both humid and dry conditions prevailed during Khabour Formation deposition, although more humid conditions indicated in the surface section may be a product of surficial weathering.

Acknowledgments

The authors thank the College of Science, University of Mosul, Iraq for administrial support. Thanks also are due to Royal Holloway University of London, UK and the Jordanian University, Jordan.

References

Akkoca DB, Karatas MA (2019). The geochemical composition of the Palu Formation from the Palu-Uluova basin, Elaziğ, Eastern Anatolia (Turkey): implication of source area, weathering, and tectonic setting. Journal of African Earth Sciences. 151: 472–489 http://doi.org/10.1016/j.jafrearsci.2019.01.007

Al Ameri T, Baban D (2002) Hydrocarbon generation potential of the lower palaeozoic succession, western Iraq desert. Iraqi Journal of Sciences. 43 (3): 77–119.

Alavi M (1980) Tectonostratigraphic evolution of the Zagrosides of Iran. Geology 8 (3):144–149

Alavi M (2007) Structures of the Zagros Fold-Thrust Belt in Iran. American Jounal of Sciences 307 (9): 1064–1095. http://doi.org/10.2475/09.2007.02

Al Fares AA, Bouman M, Jeans P (1998). A new look at the Middle to Lower Cretaceous stratigraphy, offshore Kuwait. GeoArabia, 3 (4): 543-560. https://doi.org/10.2113/geoarabia0304543

Ali S, Mohajjel M, Aswad K, Ismail S, Buckman S et al. (2014). Tectono-stratigraphy and general structure of the northwestern Zagros collision zone across the Iraq-Iran border. Jounal of Environtal Earth Sciecnce 4 (4): 92–110.

Al Hadidy AH (2007). Paleozoic stratigraphic lexicon and hydrocarbon habitat of Iraq. GeoArabia 12 (1): 63–130. http://doi.org/10.2113/geoarabia120163

Al Haj MA, Al Juboury AI, Al Hadidy AH, Hassan DK (2019). Cenomanian-early Campanian carbonate reservoir rocks of northwestern Iraq: diagenesis and porosity development. Al Kitab Journal for Pure Science, 2 (2): 1-19.

Al Harbi OA, Khan MM (2005). Mineralogy and Geochemistry of Unayzah Formation, Central Saudi Arabia: Implications for Provenance Interpretation. Journal of King Saud University (18): 35–49.

Al Harbi OA, Khan MM (2008). Provenance, diagenesis, tectonic setting and geochemistry of Tawil Sandstone (Lower Devonian) in Central Saudi Arabia. Journal of Asian Earth Sciences 33 (3-4): 278–287. http://doi.org/10.1016/j.jseaes.2008.01.004

Al Harbi OA, Khan MM (2011). Source and origin of glacial paleovalley-fill sediments (Upper Ordovician) of Sarah Formation in central Saudi Arabia. Arabian Journal of Geosciences 4 (5): 825–835. http://doi.org/10.1007/s12517-009-0097-2

Al Juboury AI (2012). A Combined Petrological-Geochemical Study of the Paleozoic Successions of Iraq. In: Al Juboury, A.I. Petrology, New Perspectives and Applications (ed.) In Tech Publishing House, Croatia, pp.169-198.

Al Juboury AI, Howard JP, Nichols G, Vincent S, Manning C et al. (2019). Sedimentology and geochemistry of potential sandstone reservoirs of the Akkas Formation, western Iraq. Journal of Petroleum Geology 42 (3): 261-280. http://doi.org/10.1111/jpg.12733

Al Juboury AI, Howard JP, Vincent SJ, Nichols G (2020). Petrography, diagenesis and geochemistry of the Cambro-Ordovician Khabour sandstones, Western Iraq: implications for reservoir quality and the impact of the Hirnantian glaciation. Marine Petroleum and Geology 123 (2): 104733 https://doi.org/10.1016/j.marpetgeo.2020.104733

Al Juboury AL, Howard JP, Vincent SJ, Nichols G (2021). Petrography, diagenesis and geochemistry of the Cambro-Ordovician Khabour sandstones, Western Iraq: Implications for reservoir quality and the impact of the Hirnantian glaciation, Marine and Petroleum Geology Elsevier, 123, https://doi.org/10.1016/j.marpetgeo.2020.104733

Amireh BS (1991). Mineral composition of the Cambrian–Cretaceous Nubian Series of Jordan: provenance, tectonic setting and climatological implication. Sedimentary Geology 71 (1-2): 99–119. https://doi.org/10.1016/0037-0738(91)90009-3

Aqrawi AAM (1998). Paleozoic stratigraphy and petroleum systems of the western and southwestern deserts of Iraq. GeoArabia 3 (2): 229–248. http://doi.org/10.2113/geoarabia0302229

Aqrawi AA, Goff JC, Horbury AD, Sadooni FN (2010). The Petroleum Geology of Iraq, Beaconsfield. Scientific Press, Bucks, UK, p. 424.

Armstrong Altrin JS, Lee YI, Kasper JJ, Carranza Edwards A, Garcia DN et al. (2012). Geochemistry of beach sands along the western Gulf, Mexico, Mexico: implication for provenance. Chemie der Erde Geochemistry 72 (4): 345–362. http://doi.org/10.1016/j.chemer.2012.07.003

Armstrong Altrin JS, Nagarajan R, Balaram V, Natalhy Pineda O (2015). Petrography and geochemistry of sands from the Chachalacas and Veracruz beach areas, western Gulf of Mexico, Mexico: constraints on provenance and tectonic setting. Journal of South American Earth Sciciences 64: 199–216. http://doi.org/10.1016/j.jsames.2015.10.012

Baban DH, Lawa FA (2016). Palynological and stratigraphical evidences on the age of the outcropped Khabour Formation near chalki nasara village, Kurdistan region, northern Iraq. Journal of Zankoy Sulaimani, Part-A- (Pure and Applied Sciences), Special Issue, GeoKurdistan II 293–318.

Bassis A (2017). Petrography, geochemistry and provenance of Saudi Arabian Palaeozoic sandstones. Technische Universität, Ph.D. Thesis, Darmstadt.

Basu A, Bickford ME, Deasy R (2016). Inferring tectonic provenance of siliciclastic rocks from their chemical compositions: A dissent. Sedimentary Geology 336, 26–35.

Basu H, Dandele PS, Kumar KR, Achar KK, Umamaheswar K (2017). Geochemistry of black shales from the Mesoproterozoic Srisailam Formation, Cuddapah basin, India: implications for provenance, palaeoweathering, tectonics, and timing of Columbia breakup. Chemie Der Erde–Geochemistry (77): 596–613.

Basu A, Young S, Suttner L, James W, Mack GH (1975). Re-evaluation of the use of undulatory extinction and crystallinity in detrital quartz for provenance interpretation. Journal of Sedimentary Petrology, 45: 873–882. https://doi.org/10.1306/212F6E6F-2B24-11D7-8648000102C1865D

Bessa AZE, Nguetchoua G, Janpou AK, El Amier YA, Nguetnga ONNM et al. (2020). Heavy metal contamination and its ecological risks in the beach sediments along the Atlantic Ocean (Limbe coastal fringes, Cameron). Earth Systems and Environment. https://doi.org/10.1007/s41748-020-00167-5

Beydoun ZR (1991). Arabian plate hydrocarbon, geology and potential: a plate tectonic approach. American Asscoaition of Petroelum Geologists Studies in Geology (33): 77.

Beydoun ZR (1993). Evolution of the northeastern Arabian Plate margin and shelf: hydrocarbon habitat and conceptual future potential. Revue de l'Institut Franc-ais du Pe'trole (48): 311–345.

Bhatia MR (1983). Plate tectonics and geochemical composition of sandstones. Journal of Geology 93 (1): 611–627.

Bhatia MR, Crook KA (1986). Trace element characteristics of graywackes and tectonic setting discrimination of sedimentary basins. Contributions to Mineralogy and Petrology (92): 181–193. http://doi.org/10.1007/BF00375292

Blanc EJP, Sherwani GM, Fouad S, Sissakian V, Vautravers BHP (2012). A Transect across the Iraqi Taurus Mountains and the Paleozoic Succession of the Khabour section, Chia Zinnar, Northern Iraq. Preliminary Field Report. : CASP, UK.

Buday T, Jassim SZ (1987). The Regional Geology of Iraq. Tectonism, magmatism and metamorphism. Geological Society of Iraq, 445pp.

Cao J, Wu M, Chen Y, Hu K, Bian LZ et al. (2012). Trace and rare earth element geochemistry of Jurassic mudstones in the northern Qaidam Basin, northwest China. Geochemistry (72): 245–252. https://doi.org/10.1016/j.chemer.2011.12.002

Chamley H (1989). Clay Sedimentology. Springer Berlin, Heidelberg, 623 pp.

Cox R, Lowe DR, Cullers RL (1995). The influence of sediment recycling and basement composition on evolution of mudrock chemistry in the southwestern United States. Geochimica et Cosmochimica Acta, (59): 2919– 2940. https://doi.org/10.1016/0016-7037(95)00185-9

Cullers RL (1995). The controls on the major and trace element evolution of shales, siltstones and sandstones of Ordovician to tertiary age in theWet Mountain region, Colorado, U.S.A. Chemical Geology (123): 107–131. https://doi.org/10.1016/0009-2541(95)00050-V

Cullers RL (2000). The geochemistry of shales, siltstones and sandstones of Pennsylvanian-Permian age, Colorado, U.S.A.: implications for provenance and metamorphic studies. Lithos 51 (3): 181–203. http://doi.org/10.1016/S0024-4937(99)00063-8

Cullers RL, Podkovyrov VN (2000). Geochemistry of the Mesoproterozoic Lakhanda shales in southeastern Yakutia, Russia: implications for mineralogical and provenance control, and recycling. Precambrian Research 104 (1): 77–93. http://doi.org/10.1016/S0301-9268(00)00090-5

Cusack M, Arrieta J M, Duarte C M (2020). Source apportionment and elemental composition of atmospheric total suspended particulates (TSP) over the Red Sea coast of Saudi Arabia. Earth Systems and Environment 4 (4): 777–788. https://doi.org/10.1007/s41748-020-00189-z

Dai S, Graham IT, Ward CR (2016). A review of anomalous rare earth lements and yttrium in coal. International Journal of Coal Geology (159): 82–95. https://doi.org/10.1016/j.coal.2016.04.005

Dickinson WR (1970). Interpreting detrital modes of graywackes and arkose. Journal of Sedimentary Petrology 40: 695–707.

Dickinson WR, Suczek CA (1979). Plate tectonics and sandstone compositions. The American Association Petroelum Geologists Bulletin 63 (12): 2164-2182. https://doi.org/10.1306/2F9188FB-16CE-11D7-8645000102C1865D

Dickinson WR, Beard LS, Brakenridge GR, Erjavec JL, Ferguson RC et al. (1983). Provenance of North American Phanerozoic sandstones in relation to tectonic setting. Geological Society of America Bulletin (94): 222–235. https://doi.org/10.1130/0016-7606(1983)94<222:PONAPS>2.0.CO;2

Floyd PA, Leveridge BE (1987). Tectonic environments of the Devonian Gramscatho basin, south Cornwall: framework mode and geochemical evidence from turbidite sandstones. Journal of the Geological Society 144 (4): 531–542. https://doi.org/10.1144/gsjgs.144.4.0531

Floyd PA, Winchester JA, Park RG (1989). Geochemistry and tectonic setting of Lewisian clastic metasediments from the early Proterozoic Loch Maree Group of Gairloch, NW Scotland.: Precambrian Research (45) 1-3: 203-214. https://doi.org/10.1016/0301-9268(89)90040-5

Folk RL (1974). Petrology of Sedimentary Rocks. Austin, TX, USA: Hemphill Publication Co. 170 pp.

Garzanti E, Padoan M, Andò S, Resentini A, Vezzoli G et al. (2013). Weathering and relative durability of detrital minerals in equatorial climate: And petrology and geochemistry in the east African rift. Journal of Geology 121: 547–580.

Ghasemlooytakantapeh S, Zohdi A, Lakirouhani A (2023). Petrography and geochemistry of the Miocene Upper Red Formation sandstones in NW Iran; with an application to the origin and tectonic setting. Marine and Petroleum Geology 153: 106275.

Ghosh S, Sarkar S (2010). Geochemistry of Permo-Triassic mudstone of the Satpura Gondwana Basin, Central India: Clues for provenance. Chemical Geolology 277: 78–100.

Haq BU, Hardenbol J, Vail PR (1987). Chronology of Fluctuating Sea Levels Since the Triassic: Science 235 (4793): 1156-1167. http://doi.org/10.1126/science.235.4793.1156

Hayashi K, Fujisawa H, Holland H D, Ohmoto H (1997). Geochemistry of ~1.9 Ga sedimentary rocks from northeastern Labrador, Canada. Geochimica et Cosmochimica Acta, (61): 4115–4137. https://doi.org/ 10.1016/S0016-7037(97)00214-7

Hussain M, Babalola LO, Hariri MM (2004). Heavy minerals in the Wajid Sandstone from Abha- Khamis Mushayt area, southwestern Saudi Arabia: implications on provenance and regional tectonic setting. GeoArabia 9 (4): 77–102. http://doi.org/10.2113/geoarabia090477

Hussain M (2001). Framework mineralogy, diagenesis and provenance of the Wajid sandstone in Asir region, Southwestern Saudi Arabia. Report, KACST Project no. LPG 283, pp. 75.

Husseini MI (1990). The Cambro-Ordovician Arabian and adjoining plates: a glacio-eustatic model: Journal of Petroleum Geology (13): 267-288. https://doi.org/10.1111/j.1747-5457.1990.tb00847.x

Husseini MI (1992). Upper Palaeozoic tectono-sedimentary evolution of the Arabian and adjoining plates: Journal of the Geological Society 149 (3): 419-429. https://doi.org/10.1144/gsjgs.149.3.0419

Ingersoll RV, Bullard TF, Ford LR, Grimm JP, Pickle JD et al. (1984). The effect of grain size on detrital modes: A test of the Gazzi-Dickinson point-counting method. Journal of Sedimentary Petrology 46: 620-632. https://doi.org/10.1306/212F83B9-2B24-11D7-8648000102C1865D

Jafarzadeh M, Shoghani Motlagh M, Mousivand F, Criniti S, Critelli S (2022). Compositional and Geochemical Signatures of Oligocene volcanoclastic sandstones of Abbasabad-Kahak area, NE Iran: Implications for provenance relations and paleogeography. Marine and Petroleum Geology 139: 105605. https://doi.org/10.1016/j.marpetgeo.2022.105605

Jassim SZ, Buday T (2006). Paleozoic Megasequences (AP1- AP5). In: Jassim SZ, Goff JC (eds) Geology of Iraq, Dolin, Prague and Moravian Museum. Dolin, Prague and Moravian Museum, Czech Republic, pp 91–103.

Jinhua FU, Shixiang LI, Liming XU, Xiaobing NIU (2018). Paleo-sedimentary environmental restoration and its significance of Chang 7 Member of Triassic Yanchang Formation in Ordos Basin, NW China. Petroelum Exploration and Developmemt. 45 (6): 98-1008.

Johnsson MJ, Stallard RF, Meade RH (1988). First-Cycle Quartz Arenites in the Orinoco River Basin, Venezuela and Colombia. The Journal of Geology, 96 (3): 263-277.

Konert G, Al Afifi AM, Al Hajri SA, Droste HJ (2001). Palaeozoic stratigraphy and hydrocarbon habitat of the Arabian plate. GeoArabia 6 (3): 407–442. http://doi.org/10.2113/geoarabia0603407

Loosveld RJH, Bell A, Terken JJM (1996). The tectonic evolution of interior Oman. GeoArabia (1): 28–51. https://doi.org/10.2113/geoarabia010128

Madhavaraju J, Ramasamy S (2002). Petrography and geochemistry of Late Maastrichtian Early Paleocene sediments of Tiruchirapalli Cretaceous, Tamil Nadue paleoweathering and provenance implications. Journal of Geological Society of India 59 (2): 133–142.

Mahdi AQ, Alshami AS, Mohammad AH, Al Tarif AM (2021). Geological, mineralogical and geochemical studies of Kolosh Formation, Dokan area, Kurdistan Region, Iraq. Al Kitab Journal for Pure Sciences, 5 (1): 39-49. https://doi.org/10.32441/kjps.05.01.p4

McCann T (1991). Petrological and geochemical determination of provenance in the southern Welsh Basin. In: Morton AC, Todd SP, Haughton PDW (eds) Developments in Sedimentary Provenance Studies 57. Geological Society London, Special Publications, pp. 215–230. https://doi.org/10.1144/GSL.SP.1991.057.01.17

McGillivray JG, Husseini MI (1992). The Paleozoic petroleum geology of central Arabia. AAPG Bulletin 76 (10): 1473–1490. https://doi.org/10.1306/BDFF8A1A-1718-11D7-8645000102C1865D

McLennan SM, Hemming S, McDaniel DK, Hanson GN (1993). Geochemical approaches to sedimentation, provenance and tectonics. In: Johnsson, M.J., Basu, A. (Eds.), Processes Controlling the Composition of Clastic Sediments, Geological Society of America Special Papers (285): 21–40. https://doi.org/10.1130/SPE284-p21

McLennan SM, Hemming SR, Taylor SR, Eriksson KA (1995). Early Proterozoic crustal evolution: Geochemical and Nd-Pb isotopic evidence from metasedimentary rocks, southwestern North America. Geochimica et Cosmochimica Acta, 59 (6): 1153–1177. https://doi.org/ 10.1016/0016-7037(95)00032-U

Nesbitt HW, Young GM (1982). Early Proterozoic climates and plate motions inferred from major element chemistry of lutites. Nature (299): 715–717.

Nesbitt HW, Young GM (1989). Formation and diagenesis of weathering profiles. Journal of Geology (97): 129–147. http://doi.org/10.1086/629290

Numan NMS (1997). A plate tectonic scenario for the Phanerozoic succession in Iraq. Journal of the Geological Society of Iraq (30): 85–110.

Nyakairu GWA, Koeberl C (2001). Mineralogical and chemical composition and distribution of rare earth elements in clay-rich sediments from Central Uganda. Geochemical Journal 35: 13–28. https://doi.org/10.2343/geochemj.35.13

Obasi RA, Madukwe HY (2016). Use of geochemistry to study the provenance, tectonic setting, source-area weathering and maturity of Igarra Marble, Southwest, Nigeria. American Journal of Engineering Research 5 (6): 90-99.

Omer MF, Friis H (2014). Cathodoluminescence investigations on quartz cement in the sandstones of Khabour Formation from Iraqi Kurdistan Region, Northern Iraq, Journal of African Earth Sciences (91): 44-54. http://doi.org/10.1016/j.jafrearsci.2020.103861

Omer MF, Friis H, Kokfelt TF, Thomsen TB (2021). Provenance of northern Gondwana Lower Ordovician sandstones (Khabour Formation, northern Iraq) revealed by detrital zircon using LA-ICP-MS dating, Geological Journal (56): 4905- 4922. http://doi.org/10.1002/gj.4210

Pettijohn FJ, Potter PE, Siever R (1987) Sand and Sandstones, New York, Springer, 553 p.

Rahman MJJ, Sayem ASM, McCann T (2014). Geochemistry and provenance of the Miocene sandstones of the Surma Group from the Sitapahar anticline, Southeastern Bengal Basin, Bangladesh. Journal of the Geological Society of India 83 (4): 447-456 http://doi.org/10.1007/s12594-014-0061-y

Roddaz M, Viers J, Brusset S, Baby P, Boucayrand C et al. (2006). Controls on weathering and provenance in the Amazonian foreland basin: insights from major and trace element geochemistry of Neogene Amazonian sediments: Chemical Geology (226): 31-65. https://doi.org/10.1016/j.chemgeo.2005.08.010

Roser BP, Korsch RJ (1986). Determination of tectonic setting of sandstone-mudstone suites using SiO2 content and K2O/Na2O ratio. The Journal of Geology 94 (5): 635–650. https://doi.org/10.1086/629071

Roser BP, Korsch RJ (1988). Provenance signatures of sandstone-mudstone suites determined using discriminant function analysis of major-element data. Chemical Geology (67): 119–139. https://doi.org/10.1016/0009-2541(88)90010-1

Saydam Eker C (2012). Petrography and geochemistry of Eocene sandstones from eastern Pontides (NE Turkey): Implications for source area weathering, provenance, and tectonic setting. Geochemistry International 50 (8): 683–701. https://doi.org/10.1134/S001670291206002X

Saydam Eker C, Korkmaz S (2011). Mineralogy and whole-rock geochemistry of late Cretaceous sandstones from the eastern Pontides (NE Turkey). Neues Jahrbuch Für Mineral Abhandlungen 188 (3): 235–256.

Saydam Eker Ç, Arı UV (2020). Geochemistry of the Middle Jurassic sediments in Gümüşhane, north-eastern Turkey: implications for weathering and provenance. Geological Journal 55: 4954–4976 https://doi.org/10.1002/gj.3726

Sengör AMC (1990). A new model for the Late Palaeozoic–Mesozoic tectonic evolution of Iran and implications for Oman. In: Robertson, A.H.F., Seale, M.P., Ries, A.C. (Eds.), The Geology and Tectonics of the Oman Region. Geological Society of London, Special Publication, 49: 797–831. https://doi.org/10.1144/GSL.SP.1992.049.01.49

Sharland PR, Archer R, Casey DM, Davies RB, Hall SH et al. (2001). Arabian Plate sequence stratigraphy. GeoArabia Special Publication 2, Gulf PetroLink, Bahrain, pp. 371.

Sissakian VK (2000). Geological Map of Iraq (Scale 1:1000000). GEOSURV, Baghdad, Iraq.

Suttner LJ, Dutta PK (1986). Alluvial sandstone composition and paleoclimate, 1. Framework mineralogy: Journal of Sedimentary Research 56 (3): 329-345. https://doi.org/10.1306/212F8909-2B24-11D7-8648000102C1865D

Taylor SR, McLennan SM (1985). The continental crust: its composition and evolution. Blackwell, Oxford, pp. 312.

Van Bellen RC, Dunnington HV, Wetzel R, Morton DM (1959). Asie, Fascicule 10a Iraq; Lexique Stratigraphic International: Paris, France, 3: 333 pp.

Verma SP, Armstrong Altrin JS (2013). New multi-dimensional diagrams for tectonic discrimination of siliciclastic sediments and their application to Precambrian basins. Chemical Geology (355): 117–133. http://doi.org/10.1016/j.chemgeo.2013.07.014

Wanas HA, Abdel Maguid NM (2006). Petrography and geochemistry of the Cambro-Ordovician Wajid Sandstone, southwest Saudi Arabia: Implications for provenance and tectonic setting. Journal of Asian Earth Sciences 27 (4): 416–429. https://doi.org/10.1016/j.jseaes.2005.05.002

Wronkiewicz DJ, Condie KC (1990). Geochemistry and mineralogy of sediments from the Ventersdorp and Transvaal Supergroups, South Africa: Cratonic evolution during the early Proterozoic. Geochimica et Cosmochimica Acta 54 (2): 343 - 354. https://doi.org/10.1016/0016-7037(90)90323-D

Wronkiewicz DJ, Condie KC (1987). Geochemistry of Archean shales from the Witwatersrand Supergroup, South Africa: Source-area weathering and provenance. Geochimica et Cosmochimica Acta. 51 (9): 2401-2416 https://doi.org/10.1016/0016-7037(87)90293-6

Zaid SM, Al Ghatani F (2015). Provenance, diagenesis, tectonic setting, and geochemistry of Hawkesbury Sandstone (Middle Triassic), southern Sydney Basin, Australia. Turkish Journal of Earth Sciences 24 (1): 72-98. http://doi.org/10.3906/yer-1407-5

Zhang Y, Wang Y, Geng H, Zhang Y, Fan W et al. (2013). Early Neoproterozoic (~850 Ma) back-arc basin in the central Jiangnan Orogen (eastern South China): geochronological and petrogenetic constraints from metabasalts. Precambrian Research (231): 325–342. http://doi.org/10.1016/j.precamres.2013.03.016

Zimmermann U, Spalletti LA (2009). Provenance of the Lower Paleozoic Balcarce Formation (Tandilia System, Buenos Aires Province, Argentina): Implications for paleogeographic reconstructions of SW Gondwana.: Sedimentary Geology (219): 7-23. https://doi.org/10.1016/j.sedgeo.2009.02.002

Zou C, Mao L, Tan Z, Zhou L, Liu L (2021). Geochemistry of major and trace elements in sediments from the Lubei Plain, China: Constraints for paleoclimate, paleosalinity, and paleoredox environment. Journal of Asian Earth Sciences 6 (1): 100071. https://doi.org/10.1016/j.jaesx.2021.100071